Experimental and Molecular Pathology 147 (2026) 105059

Contents lists available at ScienceDirect

Experimental and Molecular Pathology

journal homepage: www.elsevier.com/locate/yexmp

MicroRNAs and predicted targets in the switch from monolayered to spheroids of cholangiocarcinoma cells

Leda Roncoroni [a,b], Anna Terrazzan [c,d,*], Luca Elli [a], Pietro Ancona [c], Paula Olaizola [e], Silvia Tabano [f,g], Patrizia Colapietro [g], Filippo Gamberini [c], Chiara Orlandi [c], Gianluca Aguiari [h], Cristian Taccioli [i], Luisa Doneda [b], Nicoletta Bianchi [c]

[a] Center for Prevention and Diagnosis of Celiac Disease-Gastroenterology and Endoscopy Unit, Foundation IRCCS Ca' Granda Ospedale Maggiore Policlinico, Milan, Italy
[b] Department of Biomedical, Surgical and Dental Science, University of Milan, Milan, Italy
[c] Department of Translational Medicine, University of Ferrara, Ferrara, Italy
[d] Genomics Core Facility, Centre of New Technologies, University of Warsaw, Warsaw, Poland
[e] MRC Human Genetics Unit, Institute of Genetics and Cancer, Crewe Road South, University of Edinburgh, Edinburgh, UK
[f] Laboratory of Medical Genetics, Ospedale Maggiore Policlinico, IRCCS Ca' Granda, Milan, Italy
[g] Department of Pathophysiology and Transplantation, University of Milan, Milan, Italy
[h] Department of Neuroscience and Rehabilitation, University of Ferrara, Ferrara, Italy
[i] Department of Animal Medicine, Production and Health, University of Padua, Padua, Italy

ARTICLE INFO

Keywords:
Cholangiocarcinoma
Biliary adenocarcinoma
Spheroids
Microarray
MicroRNA
Pathways
Sk-ChA-1
Mz-ChA-1

ABSTRACT

Background: Extrahepatic cholangiocarcinoma (eCCA) is characterized by marked molecular heterogeneity and limited therapeutic options. MicroRNAs (miRNAs) are key post-transcriptional regulators of cancer-related pathways, but their contribution to tumor adaptation in physiologically relevant models remains poorly understood. Three-dimensional (3D) tumor spheroids better mimic in vivo conditions than conventional two-dimensional (2D) cultures.

Methods: We compared miRNA expression profiles in two eCCA cell lines (Sk-ChA-1 and Mz-ChA-1) grown as monolayers (2D) or multicellular tumor spheroids (3D). MiRNA profiling was performed using NanoString technology. Predicted targets were analyzed by over-representation analysis, and selected miRNAs and genes were validated by RT-qPCR and ELISA-based assays.

Results: 3D growth induced extensive miRNA remodeling, with distinct (54 deregulated in Sk-ChA-1 and 29 in Mz-ChA-1 cells) and partially overlapping signatures (miR-1283, miR-577, and miR-2113). Among the shared miRNAs, predicted targets included *DUSP10* and *RBFOX1*, while in spheroids, cell-specific multiple miRNAs converged on shared targets (*TNRC6B, SMARCAD1, ATG14, HMGA2*, and *CLOCK*) displaying inverse expression patterns. The transcriptional program impacted MAPK signaling, enhanced EMT, and activated stress-adaptive networks but attenuated proliferation in 3D Sk-ChA-1 cells, while Mz-ChA-1 cells retained a more epithelial and proliferative profile. In this context, we point out the involvement of miR-19b-3p using anti-miR transfection experiments.

Abbreviations: ADIPOR2, Adiponectin receptor 2; AKT, Protein kinase B; ATG14, Autophagy Related 14; BMPR2, Bone morphogenetic protein receptor type II; CCA, cholangiocarcinoma; CDKN1B, Cyclin-dependent kinase inhibitor 1B; circRNA, circular RNA; CLOCK, Clock Circadian Regulator; DAZ, Deleted in Azoospermia; DUSP, Dual-specificity phosphatase; eCCA, extrahepatic cholangiocarcinoma; EMT, epithelial–mesenchymal transition; E2F1, E2F transcription factor 1; ENAH, Enabled homolog actin regulator; ERK, Extracellular signal-regulated kinase; FC, fold change; FDR, false discovery rate; FIGN, Fidgetin; GLS, Glutaminase; GO, Gene Ontology; HIF1A, Hypoxia-inducible factor 1 α; HMGA2, High Mobility Group AT-hook 2; HCC, hepatocellular carcinoma; HRP, horseradish peroxidase; iCCA, intrahepatic cholangiocarcinoma; ITGB8, Integrin subunit β 8; LU, luminescence; MAPK, Mitogen-activated protein kinase; miRNA, microRNA; MCTSs, multicellular tumor spheroids; mTOR, mechanistic target of rapamycin; NANOG, Nanog homeobox; ORA, over-representation analysis; pCCA, perihilar cholangiocarcinoma; PIK3, Phosphoinositide 3-kinase; PIK3CA, Phosphoinositide 3-kinase catalytic subunit alpha; PPP2CA, Protein phosphatase 2 catalytic subunit α; PTEN, phosphatase and tensin homolog; RBFOX1, RNA binding Fox-1 homolog 1; RICTOR, RPTOR independent companion of MTOR complex 2; RORA, RAR-related orphan receptor A; RPS6KA5, Ribosomal protein S6 kinase α-5; RT-qPCR, reverse transcription–quantitative polymerase chain reaction; SKIL, SKI Like Proto-Oncogene; SLC7A11, Solute carrier family 7 member 11; TNRC6B, Trinucleotide Repeat Containing Adaptor 6B; TPM, transcripts per million; VIM, Vimentin; vs., versus; ZEB, zinc finger *E*-box binding homeobox 1.

* Corresponding author at: Department of Translational Medicine, University of Ferrara, Via Fossato di Mortara 70, 44121 Ferrara, Italy.
E-mail address: anna.terrazzan@unife.it (A. Terrazzan).

https://doi.org/10.1016/j.yexmp.2026.105059
Received 30 September 2025; Received in revised form 12 June 2026; Accepted 16 June 2026
Available online 22 June 2026
0014-4800/© 2026 Published by Elsevier Inc. This is an open access article under the CC BY-NC-ND license (http://creativecommons.org/licenses/by-nc-nd/4.0/).

Conclusion: Our findings reveal a miRNA-driven regulatory landscape associated with 3D growth in eCCA, linking tumor architecture to signaling rewiring and cellular plasticity, and highlight potentially druggable candidate targets and pathways to investigate as candidates using inhibitors or gene therapy-based interventions.

1. Introduction

Cholangiocarcinoma (CCA) represents a diverse group of malignancies originating from the ductular epithelium of the biliary tree. CCA is the second most prevalent primary liver cancer after hepatocellular carcinoma, accounting for approximately 3% of all gastrointestinal malignancies (Banales et al., 2020). Although the epidemiology of CCA varies significantly worldwide, its overall incidence is steadily increasing, posing a growing global health challenge (Khan et al., 2005). CCAs are typically asymptomatic in their early stages, leading to late and often advanced diagnoses, which severely limit therapeutic options and result in a poor prognosis (Banales et al., 2020). Based on anatomical location, CCAs can be classified as intrahepatic cholangiocarcinoma (iCCA), arising within the liver, or extrahepatic cholangiocarcinoma (eCCA), originating from the extrahepatic bile ducts. The latter can be further subdivided into perihilar cholangiocarcinoma (pCCA) and distal tumors, depending on whether they arise above or below the cystic duct. The main risk factors for CCA include chronic cholestasis, liver fluke infections, dietary nitrosamine intake, primary sclerosing cholangitis, hepatitis, cirrhosis, metabolic disorders, chronic pancreatitis, and inflammatory bowel disease (Banales et al., 2020; Khan et al., 2005; Karlsen et al., 2017; Alpini et al., 2002). This anatomical classification reflects not only differences in tumor origin but also distinct pathogenetic mechanisms, risk factors, genetic alterations, and clinical management strategies. Despite significant advances in understanding CCA over the past decade, the molecular characterization of eCCA remains limited, which in turn restricts the development of effective therapeutic strategies. Indeed, molecular targeted therapies have so far failed to demonstrate survival benefits in eCCA, likely due in part to an incomplete understanding of the underlying biological mechanisms (Montal et al., 2020). Therefore, comprehensive genomic and molecular characterization of these tumors facilitates the identification of novel therapeutic approaches (Roncoroni et al., 2008; Roncoroni et al., 2018). In this context, increasing attention has been directed toward the role of microRNAs (miRNAs) in CCA carcinogenesis (Prinz et al., 2022), where they can function either as oncogenes or tumor suppressors (Mitchell et al., 2008). MiRNAs represent ideal clinical biomarkers, as they can be isolated from plasma and serum, and are involved in key hallmarks of cancer, including invasion, metastasis, proliferation signaling, angiogenesis, apoptosis, and drug response (Mitchell et al., 2008; Schwarzenbach, 2015). Among the most extensively studied miRNAs, miR-21 plays a central role in promoting proliferation and invasion by suppressing Programmed cell death 4 and Tissue inhibitor of metalloproteinase 3 in primary CCA. In Mz-ChA-1 cells, miR-21 targets the tumor suppressor PTEN (phosphatase and tensin homolog), which is associated with the Phosphoinositide 3-kinase (PIK3)/Akt (Protein kinase B)/mammalian target of rapamycin (mTOR) signaling pathway, a cascade signaling constitutively active in many tumors and linked to enhanced cell survival (Meng et al., 2006). Additional miRNAs involved in CCA cell proliferation include miR-26a, which is associated with β-catenin–dependent gene expression in human CCA tissues and cell lines; miR-181c and miR-191, which promote cancer cell growth; and miR-494, which has been reported as a tumor suppressor biomarker (Jalil et al., 2023).

Other miRNAs, such as let-7c and miR-125b, have been shown to regulate cellular proliferation by inhibition of the IL-6/STAT3 inflammatory signaling pathway, while miR-99a exerts its effects by targeting IGF1R, modulating IGF signaling, and activating STAT3 (Isomoto et al., 2005). Activation of this cascade influences the transcriptional activity of Bcl-2 family members, thereby reducing apoptosis-dependent cell death. Consistent with its anti-apoptotic role, Bcl-2 upregulation has been associated with enhanced cell survival in CCA models, including Sk-ChA-1 and Mz-ChA-1 cell lines. Accordingly, Li et al. (2014) demonstrated that mycoepoxydiene induces apoptosis in Sk-ChA-1 and Mz-ChA-1 cells by downregulating the anti-apoptotic proteins Bcl-2 and Bcl-XL (Li et al., 2014).

Several miRNAs are downregulated in CCA, including miR-31, miR-95, and miR-125a-5p (Meng et al., 2006). MiR-31 is known to act as a tumor suppressor by interacting with p53 and E2F1 (E2F transcription factor 1) and modulating the RAS/MAPK, Transforming growth factor β, and Wnt signaling pathways (Sun et al., 2026). Similarly, miR-95 functions as a tumor suppressor by targeting Snail Family Transcriptional Repressor 2 (Zhang et al., 2019), whereas miR-125a-5p exerts oncogenic effects by targeting *TP53*-regulated inhibitor of apoptosis 1, a *TP53*-regulated gene, and B cell lymphoma-2-like protein 2 (Ming et al., 2019). Further evidence from studies conducted in six human CCA cell lines (Mz-ChA-1, TFK-1, CCLP-1, HuCC-T1, SG231, and HuH-28) and biopsy samples identified miR-34a as an antioncogene. MiR-34a specifically targets Period circadian protein homolog 1, reducing proliferation, migration, and invasion by regulation of pathways involved in cell cycle control, cell growth, and apoptosis (Han et al., 2016). In addition, miR-24, which primarily targets MEN1, has been shown to reduce proliferation, migration, and invasion in the Mz-ChA-1 cell line in both in vitro and in vivo xenograft models (Ehrlich et al., 2017).

Early studies by Meng et al. (2006) demonstrated deregulation of miR-141 and miR-200b in Mz-ChA-1 cells. MiR-141 regulates the Clock Circadian Regulator (CLOCK), a protein involved in circadian rhythm control, cell division, and apoptosis following DNA damage, whereas miR-200b targets PTEN (Isomoto et al., 2005), a protein that modulates cell transformation, growth, and cell cycle progression, and differentiation through phosphorylation of multiple substrates. Through Src-mediated activation of the Ras pathway, miR-200b enhances MAPK (mitogen-activated protein kinase) signaling, thereby promoting tumorigenic processes (Meng et al., 2006).

In this context, miR-200c upregulation is strongly associated with reduced EMT, as well as decreased migratory and invasive potential (Rupaimoole and Slack, 2017). Consistent with these findings, the clinical relevance of the miR-200 family is further supported by a recent meta-analysis by Wu et al. (2024), which evaluated the prognostic value of its members in digestive system tumors. The authors demonstrated that altered expression of miR-200 family miRNAs is significantly associated with patient survival and tumor progression, underscoring their potential role as prognostic biomarkers. Beyond their prognostic value, the miR-200 family regulates key processes including proliferation, cancer stem cell dynamics, EMT, and chemoresistance. Under physiological conditions, miR-200 family members are widely expressed and detectable in circulation. During tumorigenesis, their expression is often reduced in tissues but increased in the bloodstream, suggesting context-dependent regulation. Mechanistically, miR-200 family members directly target the 3′-UTRs of ZEB1 and ZEB2, leading to their suppression and consequent upregulation of E-cadherin, thereby maintaining the epithelial phenotype and inhibiting EMT and tumor cell migration. Conversely, ZEB1 and ZEB2 repress transcription of miR-200 genes, establishing a reciprocal regulatory loop that promotes mesenchymal traits and metastatic dissemination. These findings reinforce the importance of miR-200–mediated regulatory networks in gastrointestinal malignancies and highlight the need to further investigate their contribution to CCA biology.

Despite these advances, our current understanding of CCA-associated miRNAs remains incomplete. Expanding our knowledge of novel

miRNAs involved in the molecular mechanisms driving this aggressive and rare cancer is therefore of great interest, not only for identifying potential therapeutic agents, including miRNA agonists or antagonists, but also for uncovering druggable signaling pathways. However, most of these findings derive from conventional 2D models, which fail to fully recapitulate tumor complexity. 3D cell culture models, particularly multicellular tumor spheroids (MCTSs), are established tools in biomedical research. Compared to conventional two-dimensional (2D) cultures, spheroid-grown cells more closely resemble in vivo tumors, maintaining differentiation and functional activity. MCTSs are simplified "organ-like" structures that mimic key aspects of the tumor microenvironment, including cell–cell interactions and apical–basolateral polarity, making them valuable preclinical models (Elli et al., 2011; Roncoroni et al., 2010). Recent studies support the relevance of 3D culture systems in CCA research and their utility in modeling gastrointestinal tumors (Roncoroni et al., 2018).

Based on these considerations, we selected two CCA cell lines, Sk-ChA-1 and Mz-ChA-1, as experimental models to investigate miRNA dysregulation in MCTSs compared with canonical monolayer cultures. These cell lines are capable of aggregating into spheroids under stirring conditions, and exhibit features reminiscent of epithelial-mesenchymal transition (EMT), a process characterized by epithelial cell differentiation toward a fibroblast-like phenotype (Dolfini et al., 2005a, 2005b). EMT occurs under both physiological and pathological conditions and is associated with extensive changes in protein expression linked to cell differentiation (Dolfini et al., 2005a, 2005b; Boyer et al., 1989).

The aim of the present study was to identify novel miRNAs involved in CCA biology by comparing miRNA expression profiles in MCTSs and conventional 2D monolayer cultures. This allows the identification of both shared and cell line–specific deregulated targets, as well as markers specifically associated with the 3D model, shedding light on the molecular networks that underlie CCA progression.

2. Materials and methods

2.1. 2D and 3D cell cultures of CCA

Two eCCA cell lines were used in this study: the Sk-ChA-1 (RRID: CVCL_6952) obtained from the MRC Human Genetics Unit, Institute of Genetics and Cancer (University of Edinburgh, Edinburgh, UK), and Mz-ChA-1 (RRID:CVCL_6932) from the Center for Prevention and Diagnosis of Celiac Disease-Gastroenterology and Endoscopy Unit, Foundation IRCCS Ca' Granda (Ospedale Maggiore Policlinico, Milan, Italy). These cell lines were originally isolated by Prof. Alexander Knuth from undifferentiated and well-differentiated primary CCA of the extrahepatic bile ducts (Knuth et al., 1985). Cells were maintained in exponential growth under standard monolayer conditions and routinely checked for mycoplasma contamination. Sk-ChA-1 and Mz-ChA-1 cells were grown in DMEM (Euroclone, Milan, Italy), supplemented with 100 U/mL penicillin and 100 μg/mL streptomycin (Euroclone), 200 mM L-glutamine (Euroclone) and 10% fetal bovine serum (Euroclone). Cells were cultured in a humidified 37 °C, 5% CO_2 incubator.

MCTSs were prepared as previously described (Elli et al., 2011; Roncoroni et al., 2010). They were initiated by seeding 2.5×10^5 cells/mL in 13 mL of Iscove modified Dulbecco's medium (Euroclone), supplemented with 100 U/mL penicillin and 100 μg/mL streptomycin (Euroclone), 200 mM L-glutamine (Euroclone), 10% fetal bovine serum (Euroclone) in polycarbonate Erlenmeyer flasks (Euroclone) and incubated in a gyratory shaker (Colaver, Milan, Italy) at 60 rpm at 37 °C under atmospheric conditions. Homotypical aggregations were visible after 3 days of culture, and MCTSs were usually complete within 5 days.

2.2. Western blot analysis

Cells were lysed in buffer containing 1% Triton X-100 supplemented with a protease and phosphatase inhibitor cocktail (Sigma-Aldrich). Forty micrograms of total protein were separated on 8% SDS–polyacrylamide gels and transferred onto nitrocellulose membranes (Euroclone). Membranes were blocked for 1 h at room temperature in 5% nonfat dry milk in TBS-T (1× TBS containing 0.05% Tween-20) and incubated overnight at 4 °C with the appropriate primary antibodies diluted 1:1000 in blocking solution under constant agitation.

Primary antibodies against Akt (Catalog #9272) and phospho-Akt (Ser473, Catalog #9271), Extracellular signal-regulated kinase (ERK) 1/2 (Catalog #9102) and phospho-ERK1/2 (Thr202/Tyr204, Catalog #9101) were purchased from Cell Signaling Technology, while E-cadherin Polyclonal Antibody (Catalog #PA5–32178) was provided by Thermo Fisher Scientific. The anti-β-actin antibody (Catalog #A2228) was obtained from Merck KGaA (Germany). Enhanced chemiluminescence substrates for Western blot detection were purchased from Amersham (Milan, Italy), and horseradish peroxidase (HRP)-conjugated Anti-rabbit IgG (Catalog #7074) and Anti-mouse IgG (Catalog #7076) secondary antibodies were purchased from Cell Signaling Technology.

After washing with TBS-T, membranes were incubated for 1 h at room temperature with HRP-conjugated secondary antibodies diluted up to 1:5000. Protein bands were detected using SuperSignal™ Pico (Thermo Fisher Scientific, Milan, Italy) or ECL Select (Amersham, Milan, Italy).

Images were acquired using a ChemiDoc Imaging System (Bio-Rad, Milan, Italy) and analyzed with ImageJ software. Total protein levels and phosphorylation status were quantified by densitometric analysis and expressed as the ratio to β-actin or as the ratio of phosphorylated to total protein.

2.3. Transfection of Sk-ChA-1 monolayer cells with anti-miR™

Functional validation experiments were performed in 2D Sk-ChA-1 cells using transient transfection with specific miRNA inhibitors. Cells were transfected with Anti-miR™ miRNA inhibitors targeting hsa-miR-19b-3p (Cat. AM17000, AM10629 – MIMAT0000074) and hsa-miR-106b-5p (Cat. AM17000, AM10067 – MIMAT0000680), along with Anti-miR™ Negative Control #1 (Cat. AM17010), using Lipofectamine™ RNAiMAX (Cat. 13,778,100) according to the manufacturer's protocol. MiRNA expression levels were quantified using TaqMan™ Advanced miRNA Assays (Cat. A25576; Assay IDs 478412_mir and 478264_mir). All reagents were used following the manufacturer's instructions.

2.4. RNA extraction and purification

Total RNA, including miRNAs, was extracted using the miRNeasy MiniKit (Qiagen, Hilden, Germany), according to the manufacturer's protocol. MiRNAs were purified from total RNA using the RNeasy MinElute Cleanup Kit (Qiagen), following standard procedures, and eluted in 15 μL of RNase-free water. RNA concentration was measured using a NanoDrop spectrophotometer (ThermoFisher), and samples were stored at − 80 °C until processing.

2.5. nCounter system and NanoString technologies for miRNA profiling

The Human v3 miRNA Kit assay (NanoString technologies) was used to evaluate the expression profile of 800 human miRNAs by the NanoString platform, according to the manufacturer's instructions (NanoString technologies) and as previously described by Tabano et al., 2020. The expression profile was evaluated using approximately 100 ng of material. Each sample was analyzed in triplicate, both for 2D and 3D cell cultures. The profiling of the miRNA purified samples has been carried out using the human v3 miRNA CSO.12 assay kit (Diatech Lab Line, NanoString technologies) and the nCounter System. The data analysis was performed using nSolver Analysis Software 4.0 (https://www.nanostring.com/products/analysis-solutions/ncounteranalysis-solutions/

accessed on 28th June 2025). Before starting the analysis, we checked the quality of RNA to exclude anomalies during reactions. Sample evaluation was done applying background subtraction, geometric average of all negative and positive controls as a normalization factor, and normalization based on the codeSet content "all gene function" (excluding Housekeeping, SpikeIn, Ligation). nSolver performs a two-tailed *t*-test on the log-transformed normalized data assuming unequal variance. To account for multiple comparisons arising from the simultaneous testing of a large number of miRNAs, Benjamini–Hochberg correction was applied to control the False Discovery Rate (FDR). However, after adjustment, no miRNAs remained statistically significant (FDR = 1), likely reflecting the limited sample size and consequent reduced statistical power. Therefore, a *p*-value <0.05 was considered statistically significant, and differential expression of miRNAs in spheroids was assessed compared to the monolayered cells, applying a fold change (FC) threshold of ± 2.

2.6. Bioinformatic tools

To identify the predicted miRNA targets of each miRNA, we used the miRDB prediction algorithm (Chen and Wang, 2020) (https://mirdb.org/ accessed on 28th March 2025), using support vector machines, setting an association score $\geq$ 98% as a threshold. The list of genes obtained was used as input for Over Representation Analysis (ORA), performed with the WebGestalt web-tool (Wang et al., 2017) (https://www.webgestalt.org/ accessed on 28th June 2025). We then used Cytoscape_v3.9.0 (Shannon et al., 2003) (https://cytoscape.org/ accessed on 28th June 2025) to define the networks and NetworkAnalyst (Xia et al., 2014) (https://www.networkanalyst.ca/, accessed on 28th June 2025) to construct protein–protein interaction networks.

2.7. Validation of miRNAs using an ELISA assay system

ELISA was performed to identify and quantify miRNAs in cell lysates, based on designed probes targeting nucleic acids (specifically miR-20a-5p, miR-24-3p, miR-30d-5p, miR-155-5p, miR-146a-5p, miR-424-5p, and let-7e-5p) with high specificity and sensitivity compared to analogue methods, such as qPCR (The LIVELMIA Detection kit, BIORIDIS Srl, https://cordis.europa.eu/project/id/876715).

Probes were diluted 1:1000 in miRNA buffer to a final concentration of 5 nM. The standard curve was created after diluting the RNA standard solution 1:2000, using the Probe incubation solution, also used to resuspend 50 ng of RNA samples/100 μL per well. After 1 h of incubation at 35 °C, the solution was removed, and wells were washed five times applying 300 μL/well of Wash 2P. Then, the SA-HRP was diluted 1:100 in HRP buffer 1× to obtain the HRP-Solution, 100 μL of which were added to each well. After a 30 min incubation at room temperature with 300 rpm shaking, the solution was removed and wells washed for 5 times with 300 μL of Wash 2P and twice with 300 μL of Wash 1 T. Finally, we removed the solution, applied 100 μL/well of the substrate solution, obtained by mixing 1:1 substrate A and substrate B, and luminescence was measured within 2 min using a Tecan Infinite M200 plate reader (Tecan Group, Männedorf, Switzerland). The measurement was taken at a wavelength of 450 nm, with a secondary measurement at 540 nm used to correct for light scattering or background interference.

2.8. Detection of the levels of the predicted targets by reverse transcription-quantitative polymerase chain reaction (RT-qPCR)

Total RNA was extracted with TRIzol® Reagent (Merck KGaA), and 1 μg was reverse transcribed using TaqMan™ Reverse Transcription Reagents (Thermo Fisher Scientific) (Terrazzan et al., 2023). cDNA was amplified, and qPCR was performed at the melting temperature of 63 °C, using SYBR Green and specific primers reported in Table 1.

Relative gene expression was quantified using the comparative CT approach, in which CT values of target genes were normalized to the geometric mean of two references (β-actin and Glyceraldehyde 3-phosphate dehydrogenase) to minimize variability associated with single-gene normalization and improve accuracy and reduce variability associated with single reference genes (Vandesompele et al., 2002; Hellemans et al., 2007). FC values were then derived using the $2^{-\Delta CT}$ method. The results were analyzed with two-tailed paired Student's *t*-test considering *p*-values<0.05 as statistically significant.

Table 1
Primer sequences employed in qPCR.

Target	Primer Forward	Primer Reverse
ADIPOR2	5′- CCAAGAAGTCCGAGACACGC-3′	5′- CTGCACCCCAATCGGTTTTC-3′
ATG14	5'-TGGACTCCGTGGACGATG-3′	5'-TTCCTTCTTGTCGATAAACCTCTC-3
BMPR2	5′- AATGTCCTGGATGGCAGCA-3′	5′- CCAGCGATTCAGTGGAGATGA-3′
CD44	5'-TCCCAGACGAAGACAGTCCC-3′	5'-CCAGGTTTCTTGCCTCTTGG-3′
CDKN1B	5'-GTGCGAGTGTCTAACGGGAG-3′	5'-AGCCGGAGCCCCAATTAAAG-3′
CLOCK	5'-AAACCCCGGAGAGCGAGA-3'	5'-AGCAGCTTTGCAGGAACAAGTA-3'
E2F1	5'-CTTGGAGGGACCAGGGTTTC-3'	5'-GTTCACCTTCATTCCCCGGT-3'
ENAH	5'-TTTGTGCGAGGAGATGGTGT-3'	5′- GCAGCTCTTGCCTGACAGAT-3'
FIGN	5'-CCGCGCGTTCAGGTTAAAT-3'	5'-TGGCAGCACAAAAAGCTGAAT-3'
GLS	5′- CTGGTGGCCTCAGGTGAAAA-3'	5′- AACCTGGGATCAGACGTTCG-3'
HIF1A	5'-ACCGATTCACCATGGAGGG-3'	5'-GCCTCATCACAGAGGCCTTA-3'
HMGA2	5'-CCTAAGAGACCCAGGGGAAGA-3'	5'-GTCCTCTTCGGCAGACTCTTG-3'
ITGB8	5'-TTTCACCAGCAATGGTGCCT-3'	5'-CGGATGGCGAAAAGAGGCTA-3'
NANOG	5′- TACCTCAGCCTCCAGCAGAT-3'	5′- CTTCTGCGTCACACCATTGC-3'
PIK3CA	5'-TTTTGCTGTTCGGTGCTTGG-3'	5'-ATGCCAAAAGAAAAAGTGCCCA-3'
PTEN	5'-CTCAGCCGTTACCTGTGTGT-3'	5'-AGGTTTCCTCTGGTCCTGGT-3'
RICTOR	5′- GCCAGATTGCAGGGAGTATCA-3'	5′- CTGCTCGCACTTCTTTTGCT-3'
RORA	5′- GGAATCCGCCCGCAAGA-3'	5′- GCCCTTGCAGCCTTCACAT-3'
RPS6KA5	5′- CCCACTTATTCTCCCGCAGC-3'	5′- TCATCATTGCACTCCTGGCA-3'
SGK1	5'-GGAGGTAAACCGGGGAAACA-3'	5′- GGCTCTTGATCCACCTTCGT-3'
SKIL	5′- ACAGTCAGAGAAGGCTCACA-3'	5'-TGCAAGTGGCAGACTCAGA-3'
SLC7A11	5'-ATCTCTCCTAAGGGCGTGCT-3'	5'-TGTAGCGTCCAAATGCCAGG-3'
SMARCAD1	5'-CTTCTTTGGCCCCTTTGTGTC-3'	5'-GGGGCTTTAAATGAACTATCCAAGC-3'
TNRC6B	5'-ACTACCCAACGTCAGCCTTG-3'	5'-GCAGACCTCTCGATTGTGCT-3'
TRIM71	5'-AACAGGTGGAGATGAAGGCG-3'	5'-GGCGGATCTTTTCTACCTTCCA-3'
VIM	5'-CGTCAGCAATATGAAAGTGTGGC-3'	5'-TGTAGCGTCCAAATGCCAGG-3'
ZEB1	5'-TGCAGCTGACTGTGAAGGT-3'	5'-CCCCAGGATTTCTTGCCCTT-3'

3. Results

3.1. Cellular plasticity and signaling reprogramming induced by 3D culture

In the present study, we focused on differences between CCA cells cultured as conventional monolayers and as 3D MCTS derived from the Sk-ChA-1 and Mz-ChA-1 cell lines. The spheroidal cultures were carried out as previously detailed (Mischiati et al., 2015; Roncoroni et al., 2008). Spheroids formed through homotypical aggregation after 3–4 days and developed into stable MCTSs within 7 days, with a mean diameter of approximately 270 ± 50 μm. Morphologically, these structures showed tight cell–cell contacts, a compact outer layer, and a well-organized inner core, indicative of stable 3D organization. Previous proteomic, morphological, and functional studies performed on Sk-ChA-1 and Mz-ChA-1 MCTS have demonstrated that spheroidal growth is associated with significant phenotypic and molecular remodeling, with altered expression of adhesion- and EMT-related proteins, including reduced *E*-cadherin and increased *vimentin* (VIM), and activation of pathways related to hypoxia, metabolic adaptation, and cell survival (Mischiati et al., 2015; Roncoroni et al., 2008).

Changes in epithelial markers and MAPK-related proteins were assessed by Western blot and RT-qPCR. In Mz-ChA-1 and Sk-ChA-1 cells cultured under 2D or 3D conditions, we analyzed the phosphorylation status of Akt and ERK1/2 (extracellular signal-regulated kinases), key components of the PI3K and MAPK signaling pathways, respectively (Fig. 1, left panel). In general, Mz-ChA-1 cells exhibited higher levels of Akt and ERK1/2 phosphorylation compared to Sk-ChA-1 cells. Concerning the specific cell line, Mz-ChA-1 spheroids displayed an increase in Akt phosphorylation, although all samples started from comparable levels of total protein. Similarly, they displayed higher ERK1/2 phosphorylation, also sustained by the higher total content. In contrast, 2D and 3D Sk-ChA-1 cultures exhibited the same low Akt phosphorylation profile, whereas ERK1/2 phosphorylation was increased in spheroids, with comparable basal ERK1/2 levels.

For a deeper characterization of our spheroid model, we analyzed the expression of genes associated with key features of tumor spheroids: *VIM*, *ZEB* (zinc finger E-box binding homeobox 1), *BMPR2* (Bone morphogenetic protein receptor type II), *SKIL* (SKI Like Proto-Oncogene) and *ENAH* (enabled homolog actin regulator) among the functionally associated with VIM-high/EMT-like phenotypes, *RPS6KA5* (Ribosomal protein S6 kinase α-5) associated to MAPK signaling, *CDKN1B* (cyclin dependent kinase inhibitor 1B) and *E2F1* involved in cell cycle and proliferation, *ITGB8* (Integrin subunit β 8) as invasion-related integrin, *CD44* molecule and *NANOG* (Nanog homeobox) as markers of stemness, *RICTOR* (RPTOR independent companion of MTOR complex 2), *PIK3CA* (PIK3 catalytic subunit alpha) implicated in PI3K–mTOR/aggressiveness, *PTEN* in cell survival, *HIF1A* (Hypoxia-inducible factor 1 α), *ADIPOR2* (adiponectin receptor 2), *GLS* (glutaminase),and *SLC7A11* (solute carrier family 7 member 11) as markers of

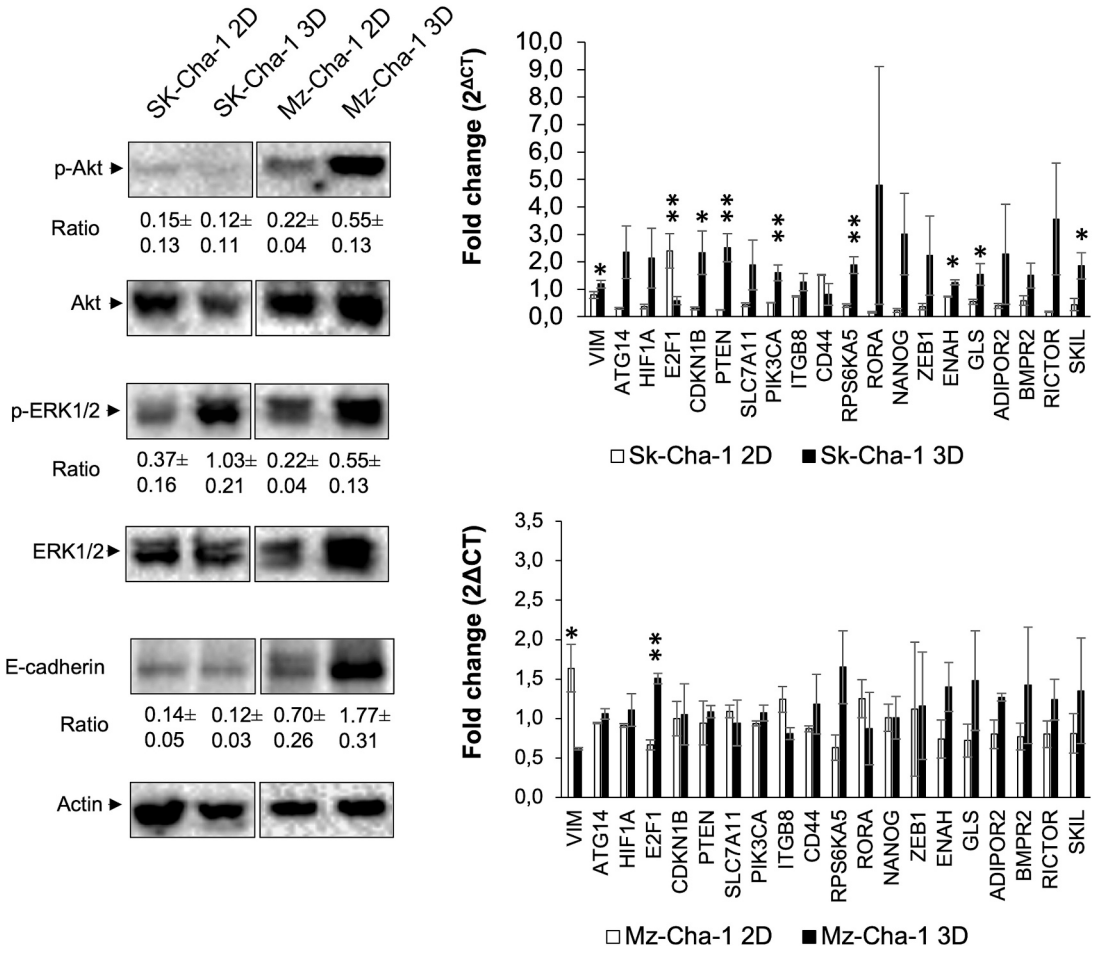

Fig. 1. Analysis of AKT/ERK pathway activation and gene expression in SK-ChA-1 and Mz-ChA-1 cells cultured under 2D and 3D conditions.
Left panel, Western blot analysis of p-AKT, AKT, p-ERK1/2, ERK1/2, and E-cadherin; actin was used as a loading control. Values indicate relative densitometric quantification from one of three independent experiments (ratios: E-cadherin/actin, p-AKT/AKT, and p-ERK/ERK). Right panel, expression of the indicated genes evaluated by RT-qPCR and reported as FC ($2^{-\Delta CT}$), normalized to the geometric mean of two reference genes, as described in Materials and Methods. The means ± standard deviation of 3 independent experiments are reported. **p*-value <0.05; ***p*-value <0.01, calculated comparing 3D vs. 2D using two-tailed Student's *t*-test.

hypoxic/metabolic adaptation, *ATG14* (autophagy related 14) for autophagy, finally *RORA* (RAR-related orphan receptor A), a regulator of metabolic and stress-adaptive transcriptional programs. In 3D cultures, we observed a general increase in most of the analyzed transcripts (Fig. 1, right panel).

With particular attention to EMT, proliferation, and cell survival, Sk-ChA-1 spheroids, in addition to exhibiting lower E-cadherin levels than Mz-ChA-1 cells (Fig. 1, right panel), showed increased *VIM* expression (Fig. 1, right panel), suggesting a shift toward a more mesenchymal and plastic phenotype. Statistically significant changes were also detected for *SKIL, ENAH, RPS6KA5, CDKN1B, PIK3CA, PTEN, GLS*, and *RORA,* except for *E2F1*. Overall, this transcriptional profile suggests enhanced EMT plasticity and activation of stress-adaptive signaling networks, including metabolic reprogramming, but attenuation of proliferation, which may depend on an increase in *CDKN1B* and a decrease in *E2F1*. The concurrent increase in *PIK3CA* and *RPS6KA5* (Fig. 1, right panel) expression and ERK activation (Fig. 1, left panel) supports the engagement of interconnected PIK3/MAPK signaling networks under 3D conditions, although Akt levels remained comparable to those in the monolayer. Concerning hypoxia, *HIF1A* expression showed an increasing trend, but its extreme variability among the spheroids did not reach statistical significance. Similar changes occurred for the invasiveness marker *CD44*.

Gene expression analysis by RT-qPCR revealed inverse regulation of *CDKN1B* and *E2F1* between Sk-ChA-1 and Mz-ChA-1 cells, indicating a partial G1 cell-cycle restraint rather than overt proliferative activation in Sk-ChA-1 cells. Moreover, *PTEN* expression was increased. This pattern is compatible with an adaptive quiescent-like state, frequently described in 3D tumor models (LaRue et al., 2004; Delarue et al., 2014).

In contrast, Mz-ChA-1 cells showed higher E-cadherin and lower *VIM* in spheroids, indicating a possible state of EMT reversion, whereas the higher levels of *E2F1* suggest a reinforcement of proliferative activity (Fig. 1).

These findings indicate distinct adaptive responses to 3D growth conditions in Mz-ChA-1 compared to Sk-ChA-1 cells, providing a relevant framework for investigating molecular regulators involved in these changes. Based on this well-established background, our work was designed to investigate whether the transition from monolayer to spheroidal growth is accompanied by specific and biologically meaningful changes in miRNA expression profiles and predicted target pathways.

3.2. *Profiling of the dysregulated miRNAs in 3D versus 2D cell cultures of CCA*

A total of 12 RNA samples were analyzed, derived from Sk-ChA-1 and Mz-ChA-1 cells cultured under 2D and 3D conditions ($n = 3$ per condition). A total of 777 miRNAs were detected by the NanoString set of probes in Mz-ChA-1 and Sk-ChA-1 cells. This list excluded those recognizing multiple miRNAs. Data from different experimental

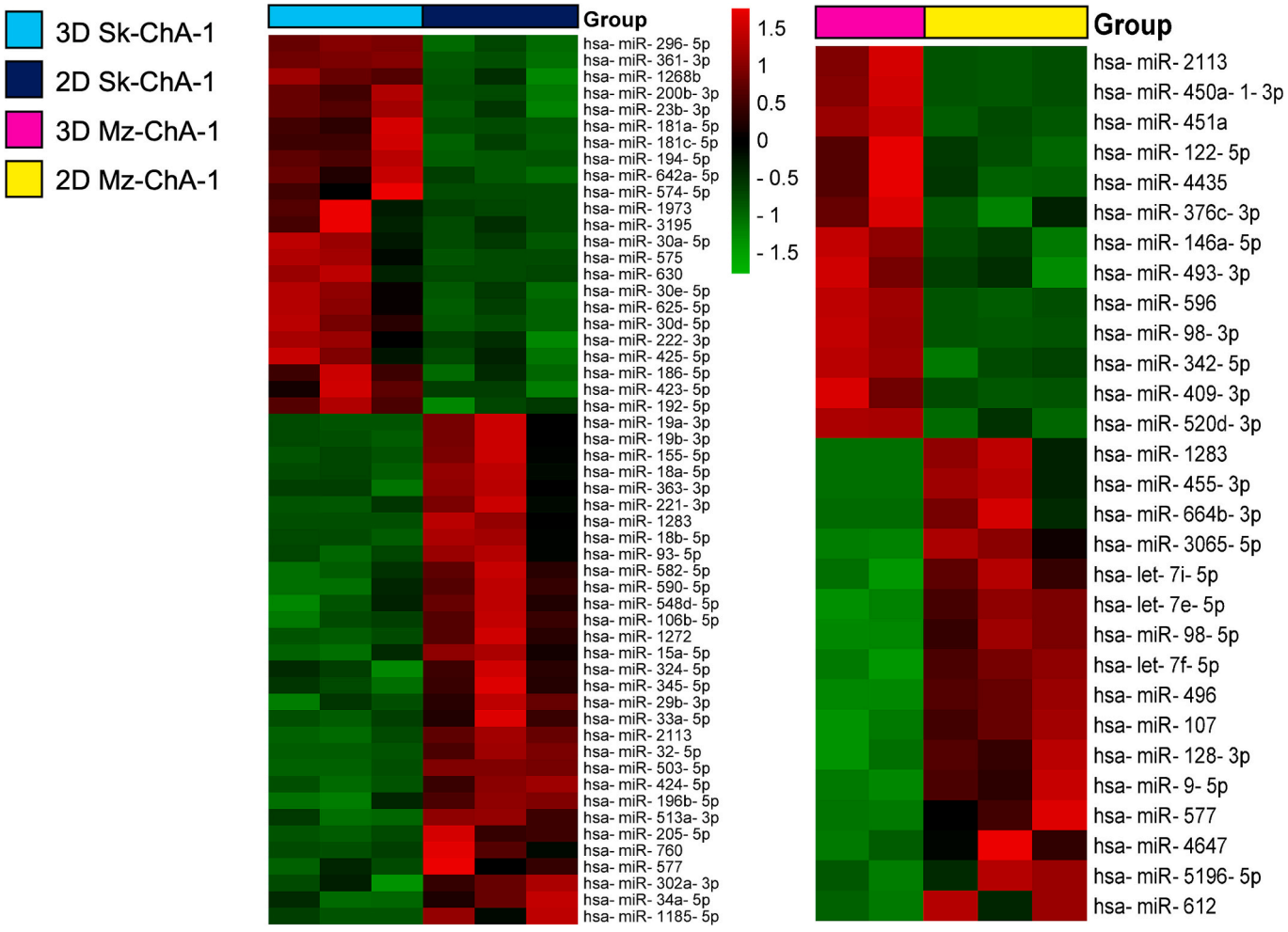

Fig. 2. Heatmaps of significantly deregulated miRNAs in 3D vs. 2D cultures of CCA cells.
Samples were analyzed using NanoString technology. Upregulated miRNAs are shown in Red, whereas downregulated miRNAs are shown in Green, selected based on FC ± 2 (p-value <0.05). The figure was created with SRplot web-based tool. (For interpretation of the references to colour in this figure legend, the reader is referred to the web version of this article.)

conditions, spheroids versus (vs.) monolayer, of each cell line were analyzed using nSolver® v4.0 software, by applying the Euclidean distance method and the average linkage for clustering (p-value <0.05, obtained using two-tailed t-test and unequal variance). One 3D Mz-ChA-1 sample did not pass the software quality control, hence it was discarded for the subsequent analysis. After exclusion, the 3D Mz-ChA-1 group included two samples ($n = 2$), reducing statistical power. Using a fold change (FC) threshold of ±2, we identified 54 miRNAs in Sk-ChA-1 (31 down- and 23 up-regulated) and 29 miRNAs (16 down- and 13 up-regulated) in Mz-ChA-1 cells, as reported in Fig. 2.

A Venn diagram (Fig. 3) shows both the common miRNAs dysregulated in 3D vs. 2D cell lines and the significantly altered miRNAs associated with a specific culture condition. Despite the large number of deregulated miRNAs, we identified three common miRNAs, miR-1283, miR-577, and miR-2113. The first two were downregulated in both spheroid cells, while miR-2113 was upregulated in Mz-ChA-1 spheroids and downregulated in Sk-ChA-1 spheroids. The remaining miRNAs were specific to each cell line and culture condition as reported in Table S1. Hierarchical clustering and heatmap are reported in Fig. S1.

We selected a list of highly deregulated miRNAs for further validation, including miR-20a-5p, miR-24-3p, miR-30d-5p, miR-155-5p, miR-146a-5p, miR-424-5p, and let-7e-5p. An ELISA-based assay was used to validate the microarray results. The platform LIVELMIA® developed by BIORIDIS represents a probe-based hybridization assay coupled to enzymatic signal amplification, allowing direct quantification of mature miRNAs without reverse transcription. In Fig. 4, the results of a triplicate analysis for each experimental condition are reported, confirming NanoString results for miR-20a-5p, miR-146a-5p, and miR-30d-5p in both cell lines, while miR-24-3p was used as a reference, given its steady expression across conditions. Notably, we observed upregulation of miR-30d-5p in Sk-ChA-1 spheroids (p-value <0.05), further confirming the NanoString data.

3.3. Biological functions of target genes linked to the three common deregulated miRNAs

We analyzed the possible biological roles of the predicted targets (with a score of ≥98% according to the miRDB database) of the dysregulated miRNAs shared by both cell lines. An ORA was performed by the

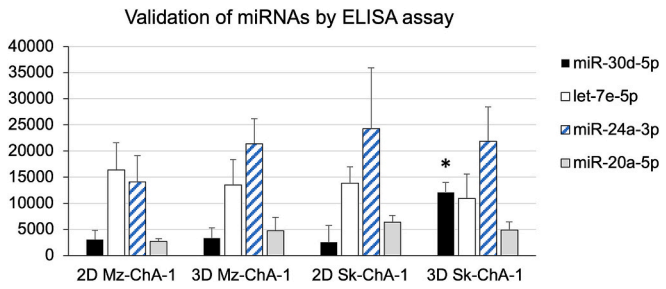

Fig. 4. Validation of selected miRNAs by ELISA assay.
Quantification was performed using specific miRNA probes associated with a biotin–streptavidin system and HRP. Luminescence (LU) was measured using a Tecan Infinite M200 reader (Tecan Group). Three samples from each culture condition and cell line were analyzed. All measurements were performed in triplicate (*, p-value <0.05, calculated comparing 3D vs. 2D using two-tailed Student's t-test).

Gene Enrichment tool of the WEB-based GEne SeT AnaLysis Toolkit (WebGestalt). Two significantly enriched categories (FDR ⩽ 0.05), "translation regulator activity" (GO:0045182) and "mRNA binding" (GO:0003729) belonging to "no redundant Molecular Function", were identified using the gene ontology (GO) (Fig. 5). The first category includes interesting genes, such as the cytoplasmic protein Tripartite motif containing 2 and four genes of the Deleted in Azoospermia family (*DAZ1, DAZ2, DAZ3*, and *DAZ4*). In the "mRNA binding" category, we found three noteworthy genes: Nuclear cap binding protein subunit 1, RNA binding Fox-1 homolog 1 (*RBFOX1*, *alias A2BP1*), and Serine/Arginine-rich splicing Factor 1. DAZ proteins bind to the 3'-UTR of mRNA molecules involved in cell division, while the others are engaged in the stabilization and processing of transcripts (Kang et al., 2015).

Interestingly, Kaplan–Meier analysis using a web-based tool and TCGA data (UALCAN portal, accessed on 5th July 2025, Chandrashekar et al., 2022) revealed a statistically significant association between low survival and high expression of *DAZ1* and *RBFOX1*, predicted targets of miR-577 (Fig. 6). While *DAZ1* expression is higher in normal and stage I samples, *RBFOX1* is more strongly expressed in tumor tissues, particularly in stage IV disease. This trend, consistent with the downregulation

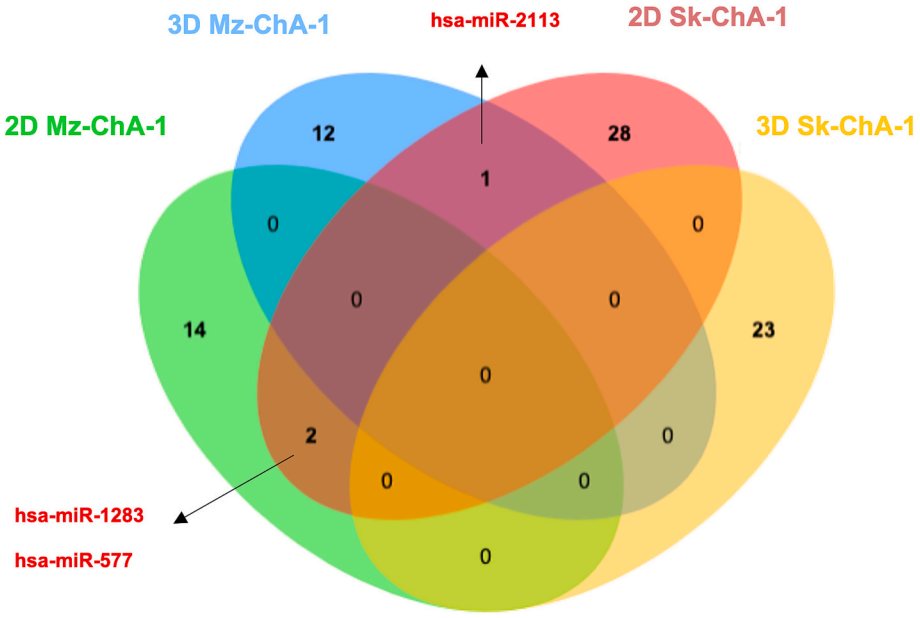

Fig. 3. Venn diagram of deregulated miRNAs in cholangiocarcinoma cells.
Colored sets represent miRNAs uniquely or commonly expressed across different cell lines and culture conditions. Common miRNAs are shown in the overlapping regions. The figure was created with SRplot web-based tool.

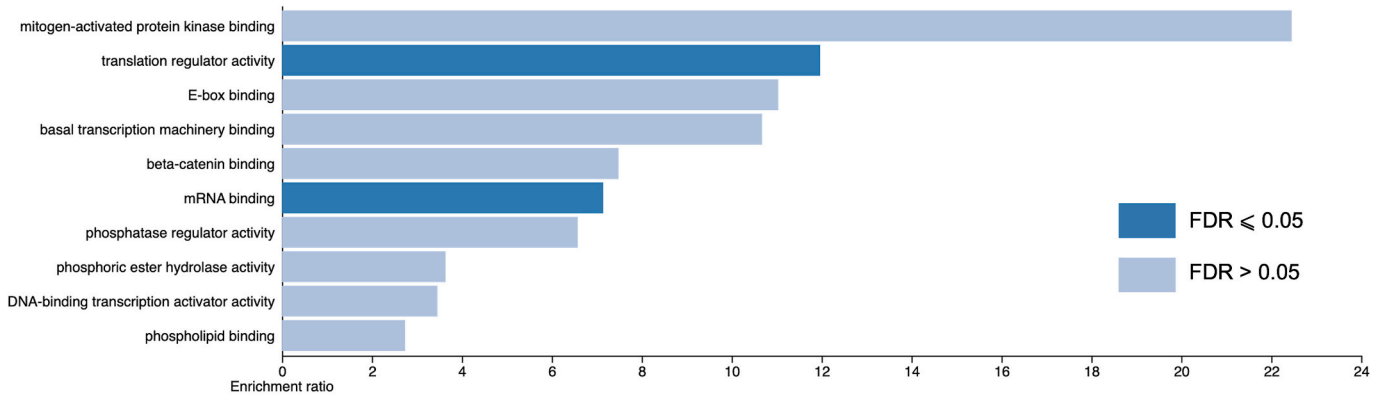

Gene Set	Description	Gene set size	Expected Value	Overlap	Enrichment Ratio	*p*-value	FDR	Genes Overlapping
GO:0051019	mitogen-activated protein kinase binding	29	0.182	2	22.455	0.0035434	0.32835	DUSP10; DUSP16
GO:0045182	translation regulator activity	136	0.271	5	11.971	0.000056578	0.0078643	DAZ1; DAZ2; DAZ3; DAZ4; TRIM2
GO:0070888	E-box binding	59	0.062	2	11.037	0.014092	0.69565	PTF1A; TCF4
GO:0001098	basal transcription machinery binding	61	0.154	2	10.675	0.015014	0.69565	TCF4; ZNF326
GO:0008013	beta-catenin binding	87	0.163	2	7.4851	0.029198	1	AMER2; TCF4
GO:0003729	mRNA binding	319	0.577	7	7.1448	0.000046069	0.0078643	DAZ1; DAZ2; DAZ3; DAZ4; NCBP1; RBFOX1; SRSF1
GO:0019208	phosphatase regulator activity	99	0.718	2	6.5778	0.037002	1	PPP1R26; PPP4R2
GO:0042578	phosphoric ester hydrolase activity	358	0.321	4	3.6380	0.023556	0.93552	DUSP10; DUSP16; PPP2CA; PTPRC
GO:0001216	DNA-binding transcription activator activity	471	1.141	5	3.4565	0.014040	0.69565	CASZ1; PTF1A; RBPJ; TCF4; TFAP2A
GO:0005543	phospholipid binding	476	1.369	4	2.7361	0.057196	1	AMER2; GOLPH3; MTSS1; PIK3C2A

Fig. 5. Molecular functions associated with commonly deregulated miRNAs in cholangiocarcinoma cells.
ORA was performed based on the predicted target genes of miR-1283, miR-577, and miR-2113 using the "Gene Ontology – Molecular Function (non-redundant)" database. Results are displayed as bar plots. Blue bars indicate gene sets and categories with FDR⩽ 0.05. The lower panel reports additional parameters, including statistical significance. The figure was generated using WebGestalt. (For interpretation of the references to colour in this figure legend, the reader is referred to the web version of this article.)

of miR-577, suggests a possible role of *RBFOX1* as a marker of poor survival for patients with higher levels of expression. Cytoscape was used to construct interaction networks. We created interaction networks, the miRNAs as "source nodes" and the genes as "target nodes", assigning a directionality to the graph (Fig. S2). This approach generated miRNA–target interaction networks. Notably, although no shared target genes were identified, Reactome pathway analysis revealed enrichment in "Reactome Pathways", we found an enrichment in the "signaling by MAPK mutants" (REAC:R-HSA-9652817) and "negative regulation of MAPK pathway" (REAC:R-HSA-5675221) terms, including targets such as Dual-specificity phosphatase 10 and 16 (*DUSP10* and *DUSP16*) (Zhou et al., 2023), *ADIPOR2* and Protein phosphatase 2 catalytic subunit α (*PPP2CA*), recognized by miR-1283 and miR-2113, whereas DAZ family members were predicted targets of miR-577.

Since miRNA–target interactions and pathway enrichments were derived from in silico prediction tools and over-representation analyses, these findings should be considered hypothesis-generating and will require direct mechanistic validation in future studies.

3.4. Biological functions of the target genes associated with the dysregulated miRNAs characterizing each cell line

To analyze the potential role of cell line-specific miRNAs, we used the previously described webtools and focused on the predicted targets with a confidence score ⩾ 98%. In Mz-ChA-1 cells, we identified the previous enriched GO molecular function categories (FDR⩽ 0.05), "translation regulator activity" (GO:0045182) and "mRNA binding" (GO:0003729), including 4 and 9 overlapping genes (Fig. 7A), respectively. In the case of Sk-ChA-1 cells, we discovered a higher number of significantly enriched GO molecular function categories, such as "mRNA binding", "beta-catenin binding", "DNA-binding transcription activator and repressor activity", "Histone modifying activity", and "protein serine and serine/threonine kinase activity" (Fig. 7B), consistent with the higher number of deregulated genes in this cell line.

We then focused on the miRNAs sharing predicted target genes (evidenced in the gene sets of the GO, in Table S1). In Sk-ChA-1 spheroids, the upregulated miR-30a-5p, miR-30d-5p, and miR-30e-5p shared 86 predicted target genes; the upregulated miR-181a-5p and miR-181c-5p had 60 common targets, while the downregulated miR-19a-3p and miR-19b-3p shared 59 targets; finally, the downregulated miR-221-3p and upregulated miR-222-3p had 7 common targets. In Mz-ChA-1 spheroids, the downregulated let-7e-5p, let-7f-5p, and let-7i-5p and upregulated miR-98-5p recognized 22 predicted targets.

Since we were interested in genes targeted by multiple miRNAs, we selected a set of candidate genes, including: Tripartite Motif Containing 71 (*TRIM71*), an evolutionary conserved RNA-binding protein; *SMARCAD1*, encoding a helicase and ATP-dependent histone octamer exchange factor associated with genetic instability; High Mobility Group AT-hook 2 (*HMGA2*), a small nonhistone chromatin-associated protein; *CLOCK*, a transcription factor known to influence both the persistence and the period of circadian rhythms; Trinucleotide Repeat Containing Adaptor 6B (*TNRC6B*), capable of binding RNA and involved in the regulation of gene expression; Autophagy Related 14 (*ATG14*), an autophagy regulatory factor associated with Beclin-1; Fidgetin (*FIGN*), a

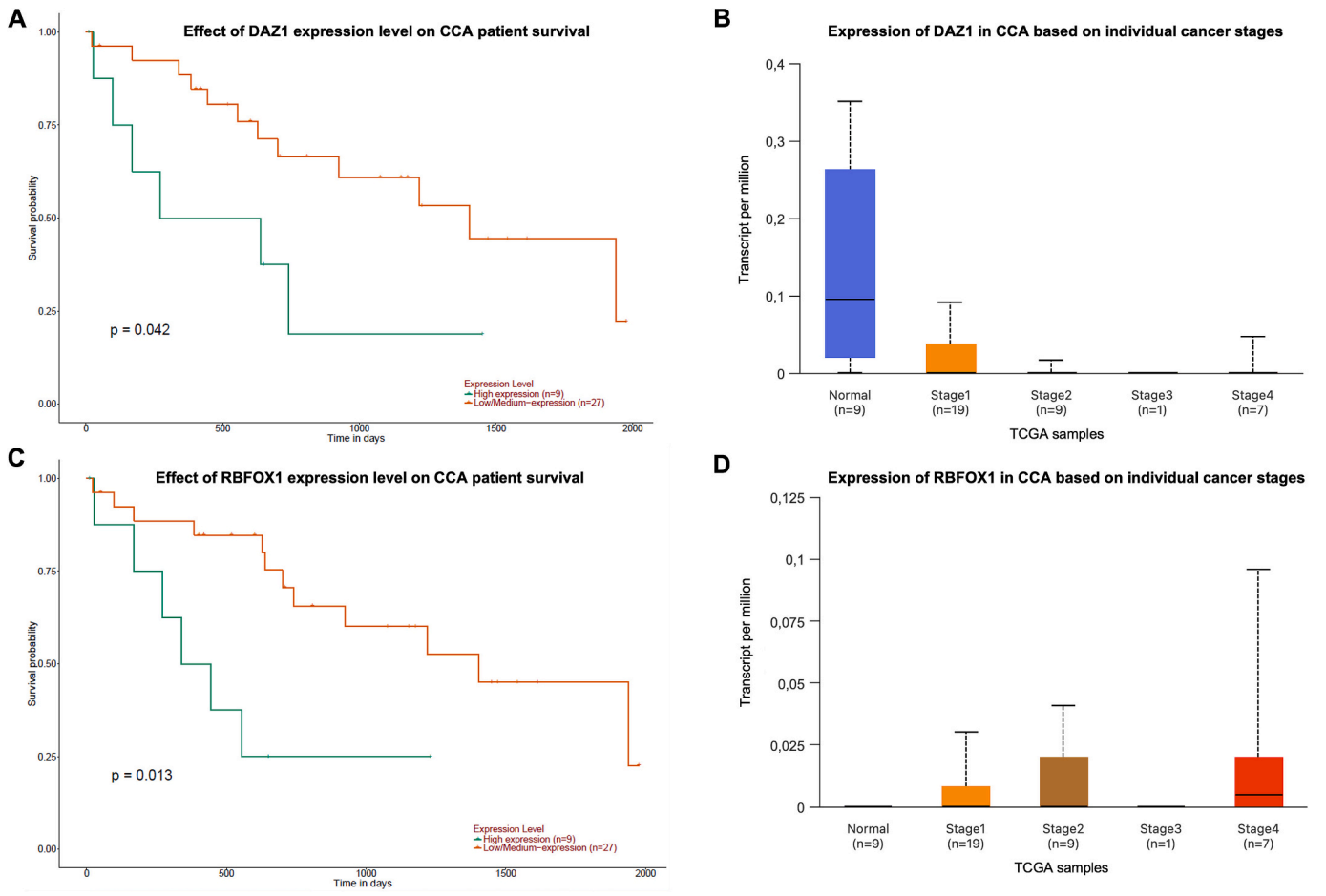

Fig. 6. Kaplan–Meier survival curves and expression levels of *DAZ1* and *RBFOX1*.
Survival curves for *DAZ1* (A) and *RBFOX1* (C) in patients with cholangiocarcinoma were generated using the UALCAN Data Analysis Portal accessed on 5th July 2025 (Chandrashekar et al., 2022). Survival probability is shown on the y-axis and time on the x-axis. High expression levels are indicated in green, whereas low/medium levels are shown in Red. Both genes show statistically significant differences (p-value = 0.042 and p-value = 0.013, respectively). mRNA expression levels of *DAZ1* (B) and *RBFOX1* (D), expressed as transcripts per million (TPM), in normal tissues and cholangiocarcinoma (CHOL) samples stratified by pathological stage. Data were obtained from the TCGA cohort. Box plots represent the median and interquartile range, with whiskers indicating minimum and maximum values. (For interpretation of the references to colour in this figure legend, the reader is referred to the web version of this article.)

negative regulator of microtubule growth. We analyzed their expression by RT-qPCR and predicted miRNAs using Nanostring. The results were reported in Fig. 8A and Fig. 8B, respectively. We found that *TNRC6B* was inversely correlated with miR-19a-3p and miR-19b-3p in both cell lines. In contrast, *CLOCK* and *ATG14* were altered only in Sk-ChA-1 cells, in which *SMARCAD1* and *HMGA2* were also modulated in accordance with let-7i-5p levels. Treatment of 2D Sk-ChA-1 cells with anti-miR-19b-3p resulted in significant upregulation of circadian-related transcripts, most notably *CLOCK*, as shown in Fig. 8C. Interestingly, *VIM* and *BMPR2*, associated with a role in EMT-like plasticity and adaptation to the tumor microenvironment, were also upregulated by treatment.

We validated our results using in vivo data from the CHOL cohort (n, normal = 9) and primary CCA (n = 36 tumor samples) from the TCGA database, by comparing the expression of our panel of genes. Using GEPIA2 (Tang et al., 2019) (http://gepia2.cancer-pku.cn/, last accessed on 5th September 2025), we observed a statistically significant difference in our signature panel between normal and tumor samples (p-value <0.01, $Log_2FC = 1$, Fig. 9A). Our results are consistent with the expression patterns of the same genes reported in TCGA (Fig. 9B).

4. Discussion

Evaluating the miRNA landscape in CCA provides valuable insights into tumor biology, as miRNAs regulate key processes such as proliferation, apoptosis, EMT, and therapy resistance, and may serve as both diagnostic and prognostic biomarkers. Our analysis focused on two CCA cell lines, Sk-ChA-1 and Mz-ChA-1, representing the eCCA subtype, which remains particularly challenging due to its poorly characterized molecular features and limited therapeutic options (Montal et al., 2020).

A previous extensive characterization of this MCTS model (Mischiati et al., 2015; Roncoroni et al., 2008) provides a solid biological framework to investigate the modulation of miRNAs in the context of tumor adaptation and aggressiveness, focusing on the signaling cascade and EMT features. Mz-ChA-1 cells displayed higher basal levels of Akt and ERK1/2 phosphorylation than Sk-ChA-1 cells, with 3D cultures enhancing activation of these pathways, especially ERK1/2 phosphorylation. Both the PI3K/AKT and MAPK/ERK pathways are frequently altered in CCA and represent a well-established driver of progression and therapeutic resistance (Yang et al., 2024). In particular, spheroids modulated oncogenic signaling in a strongly cell line–dependent manner, highlighting intrinsic phenotypic differences between these two cellular models. For example, the transcripts encoding CDKN1B and E2F1 showed opposite regulation in the shift to 3D cultures. The concurrent increase in ERK1/2 phosphorylation supports the activation of pro-survival networks in 3D Sk-ChA-1, despite exhibiting features linked to lower proliferative activity. Indeed, the upregulation of *CDKN1B* together with reduced *E2F1* expression suggests partial G1 restraint, a condition suggesting a pro-survival state. Overall, the transcriptional

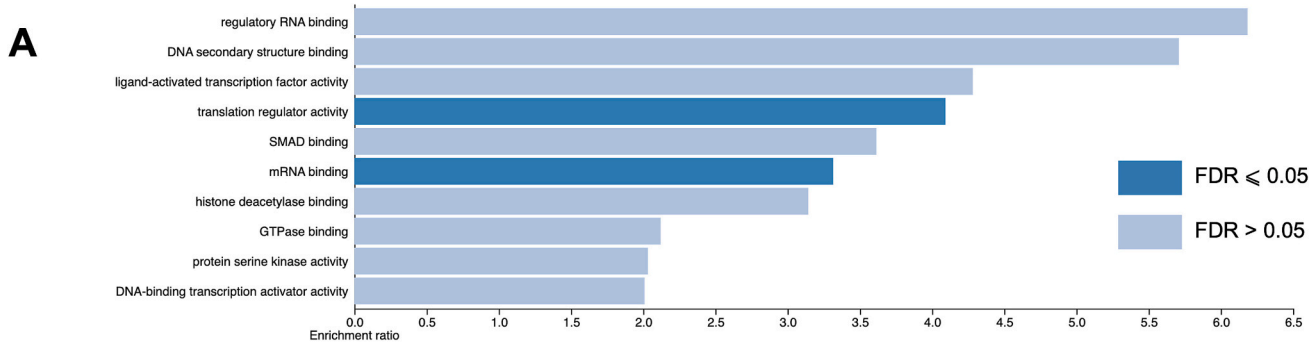

Gene Set	Description	Gene set size	Expected Value	Overlap	Enrichment Ratio	*p*-value	FDR
GO:0003729	mRNA binding	319	5.7314	19	3.3151	0.0000049382	0.0013728
GO:0045182	translation regulator activity	136	2.4435	10	4.0925	0.00017029	0.023670

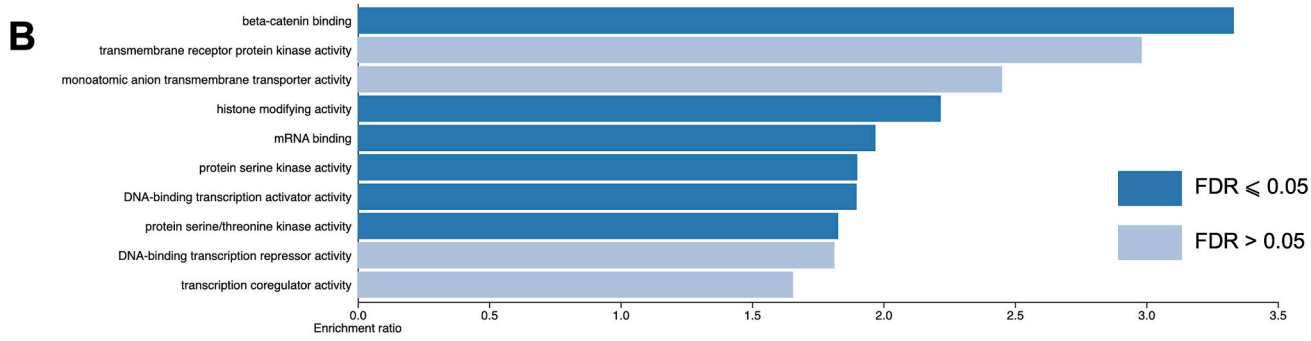

Gene Set	Description	Gene set size	Expected Value	Overlap	Enrichment Ratio	*p*-value	FDR
GO:0001216	DNA-binding transcription activator activity	471	19.492	37	1.8982	0.00013815	0.032403
GO:0008013	beta-catenin binding	87	3.6005	12	3.3329	0.00023311	0.032403
GO:0004674	protein serine/threonine kinase activity	423	17.506	32	1.8280	0.00073992	0.045231
GO:0003729	mRNA binding	319	13.202	26	1.9694	0.00077882	0.045231
GO:0106310	protein serine kinase activity	356	14.733	28	1.9005	0.00086530	0.045231
GO:0140993	histone modifying activity	207	8.5667	19	2.2179	0.00097620	0.045231

Fig. 7. Molecular functions of predicted targets of unique miRNAs in Mz-ChA-1 cells (A) and Sk-ChA-1 cells (B).
ORA was performed using the "Gene Ontology – Molecular Function (non-redundant)" database. Results are displayed as bar plots. Blue bars indicate GO categories with FDR⩽ 0.05. The lower panel reports additional parameters, including statistical significance. The figure was generated using WebGestalt. (For interpretation of the references to colour in this figure legend, the reader is referred to the web version of this article.)

profile of Sk-ChA-1 spheroids is consistent with enhanced epithelial-mesenchymal plasticity and activation of stress-adaptive programs, suggesting a metabolically flexible and potentially more aggressive tumor-like state. On the other hand, increased *VIM* and decreased E-cadherin indicate the activation of the EMT program, which may reflect a survival–plasticity state commonly associated with microenvironmental adaptation in solid tumors. The differential expression of E-cadherin observed between Sk-ChA-1 and Mz-ChA-1 cells further underscores the heterogeneity of epithelial plasticity in CCA models. E-cadherin is a hallmark whose loss correlates with EMT, which is currently recognized as a dynamic and reversible spectrum rather than a binary switch. In this context, the higher E-cadherin expression detected in Mz-ChA-1 cells, despite their stronger activation of AKT and ERK signaling, suggests that enhanced oncogenic pathway activation does not necessarily correspond to a fully mesenchymal phenotype. Mz-ChA-1 spheroids maintain a more epithelial-like and proliferative phenotype, while Sk-ChA-1 spheroids adopt a more plastic, survival-oriented configuration, with moderate enhancement of pro-growth pathways. These differences likely reflect the distinct intrinsic wiring of oncogenic networks between these two models. Together, these findings highlight a complex interplay between PI3K/AKT–MAPK signaling and plasticity in eCCA, reinforcing the idea that signaling activation and epithelial identity are not linearly correlated but context-dependent, in agreement with the marked molecular heterogeneity of CCA and in vitro models (Banales et al., 2020). These findings underscore the pivotal role of model selection in reliably dissecting disease mechanisms and revealing actionable therapeutic vulnerabilities.

From this point of view, miRNA profiling can provide a rational basis for future functional studies.

Notably, Sk-ChA-1 cells harbor a *KRAS* mutation (COSMIC entry: COSS924011), while both Sk-ChA-1 and Mz-ChA-1 carry *CDKN2A* mutations (COSMIC entry: COSS924011; COSS927192). Activating *KRAS* mutations not only drive canonical MAPK/ERK and PI3K/AKT signaling (Prior et al., 2012; Simanshu et al., 2017) but also reshape post-transcriptional regulatory networks mediated by miRNAs (Bortoletto and Parchem, 2023). Emerging evidence indicates that mutant KRAS can globally influence miRNA expression profiles, including miRNA biogenesis and functional activity (Shi et al., 2021), thereby promoting malignant phenotypes such as enhanced proliferation, invasiveness, and survival. Notably, the interaction between KRAS and miRNAs is bidirectional: while several miRNAs directly target KRAS (Chhichholiya et al., 2024), oncogenic KRAS can in turn alter miRNA processing and suppress global miRNA function (Shui et al., 2023), contributing to widespread transcriptomic deregulation and therapeutic resistance.

Concerning the loss of CDKN2A function, a key tumor suppressor gene encoding p16ˆINK4a and p14ˆARF (Sherr, 2001), critical regulators of cell cycle progression and the G1/S checkpoint, it leads to uncontrolled cell cycle entry and contributes to tumor progression. Although the direct link between *CDKN2A* mutations and miRNA profiles is less well characterized than that of *KRAS*, accumulating evidence suggests

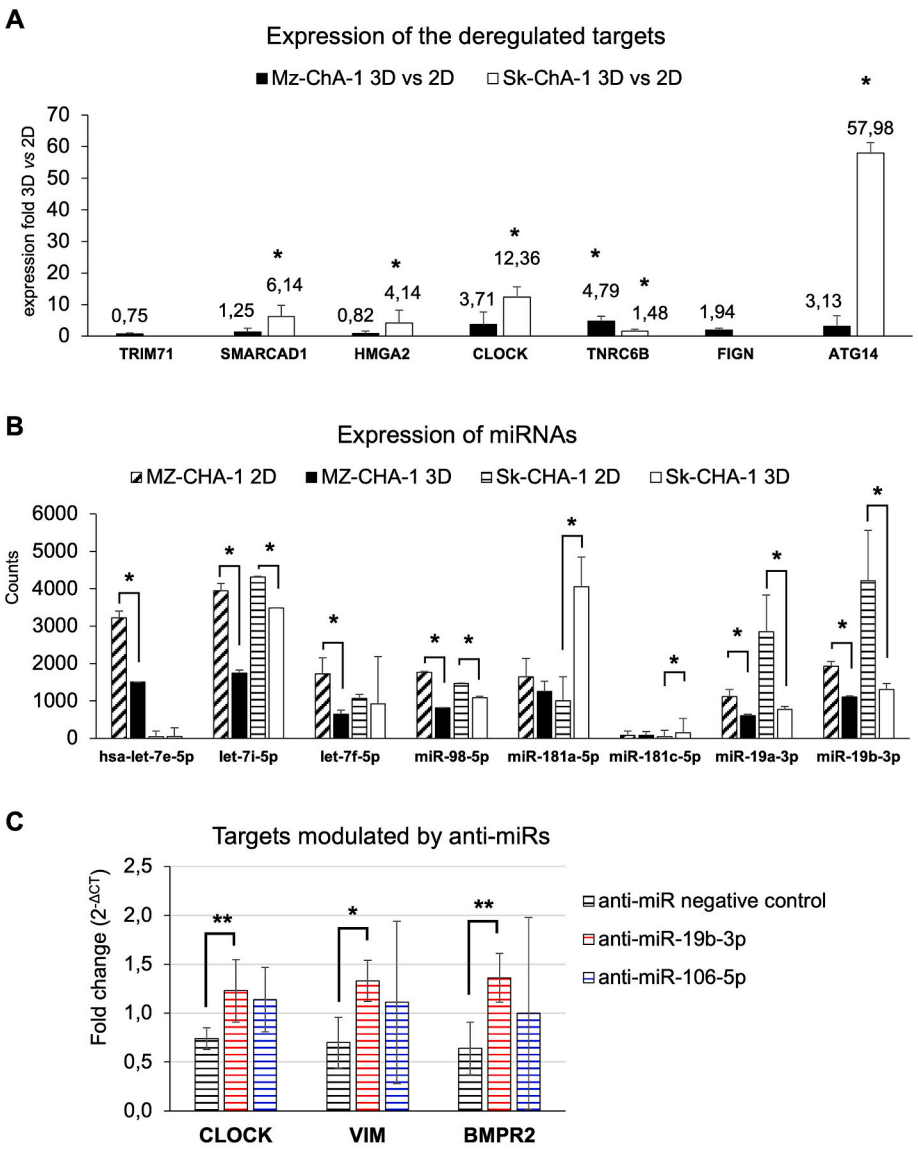

Fig. 8. Expression of Genes targeted and miRNAs comparing 3D vs. 2D cultures.
(A) Gene expression levels were determined by RT-qPCR and (B) miRNA expression levels were assessed by NanoString technology and reported as counts (*p-value <0.05, two-tailed Student's t-test). (C) Effects of anti-miR-19b-3p transfection in Sk-ChA-1 cells. RT-qPCR analysis showed modulation of selected target and EMT-associated genes compared to cells treated with a negative anti-miR or an unrelated miR-106-5p, taken as controls. All measurements were performed in triplicate (*p-value <0.05, **p-value <0.01; Welch's t-test).

functional interplay between CDKN2A-controlled pathways and miRNA regulation. Indeed, several miRNAs have been reported to target *CDKN2A* or modulate downstream ERK/JNK/MAPK signaling in specific types of tumors (Sadeghi et al., 2026).

Based on these findings, the observed 3D-specific miRNA signatures could be partially modulated by these intrinsic genomic backgrounds, potentially amplifying or attenuating pathway-related effects. Moreover, these mutations have been associated with drug resistance in CCA (DiPeri et al., 2024), so they could represent new druggable targets for miRNA therapies (Hu et al., 2019).

As the cell lines considered in this study contain the same mutation in 2D and 3D cultures, we believe that miRNAs consistently deregulated may be more likely influenced by 3D regulatory programs rather than mutation-specific effects.

Regarding the shared miRNAs, we found that miR-2113 is inversely regulated between these two models. In hepatocellular carcinoma (HCC), miR-2113 overexpression inhibited cancer growth and EMT, targeting WDR66 and interfering with eIF4AIII (Zhang et al., 2020). This is consistent with the different expressions of *E2F1* and *VIM* observed in these eCCA cell lines. This miRNA is also strictly associated with the modulation of *CDKN2A* in several cancers (Han et al., 2022; Arnoff and El-Deiry, 2022), a gene mutated in Mz-ChA-1. MiR-2113 may therefore contribute to the distinct phenotypic behaviors observed between the two models. In contrast, miR-577 and miR-1283 decreased in both 3D cultures. Notably, the *ENAH* transcript is directly involved in actin cytoskeleton remodeling and cell motility and is indirectly associated with EMT-related and VIM-high phenotypes. It was significantly upregulated in spheroids of Sk-ChA-1, also showing an inverse relationship with predicted miR-1283 expression. Low levels of miR-1283 are reported to be linked to cell proliferation in glioma, via modulation of activating transcription factor 4 (Chen et al., 2019). MiR-1283 levels could be regulated by circular RNAs (circRNAs) working as sponges in different tumors (Li et al., 2022; Yu et al., 2022). Similarly, miR-577 is under the control of circRNA (Qian et al., 2023), and its lower expression correlates with EMT (Yin et al., 2018) and cancer progression, affecting Wnt signaling (Zhang et al., 2016).

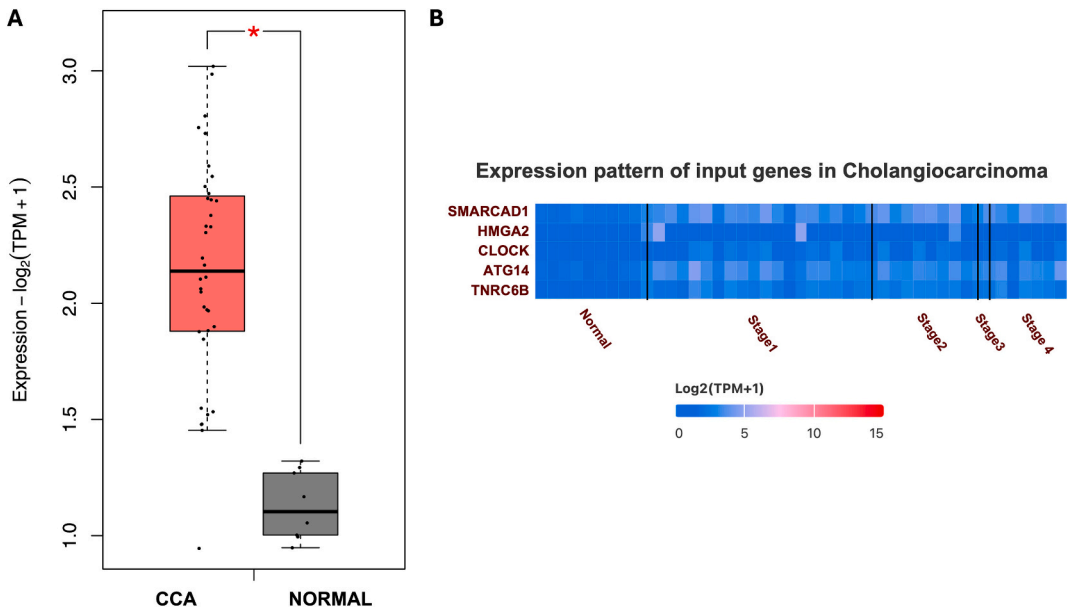

Fig. 9. Differential expression of selected genes in cholangiocarcinoma vs. normal samples.
(A) Box plot showing expression differences between normal (Grey) and tumor (Red) samples for the selected gene panel (*SMARCAD1, HMGA2, ATG14, CLOCK*, and *TNRC6B*). Red asterisks indicate statistically significant differences (*p-value <0.01). Box plots represent the median and interquartile range, with whiskers indicating minimum and maximum values. (B) Heatmap generated using the UALCAN Data Analysis Portal, accessed on 5th July 2025 (Chandrashekar et al., 2022), showing expression of the selected genes from the validated dataset (p-value <0.05). Gene expression is reported as log2(TPM + 1). (For interpretation of the references to colour in this figure legend, the reader is referred to the web version of this article.)

Overall, the low expression of miR-1283 and miR-577 may be candidate markers of changes associated with a shift of CCA toward a more invasive phenotype, comparable to the MCTSs employed in this study. In general, the predicted genes targeted by the three common miRNAs were involved in splicing, stabilization, and regulation of translation processes of transcripts that impact cell division. In this context, *DAZ1* and *RBFOX1*, putative targets of miR-577, correlated with low survival rates in patients with CCA, as indicated in the Kaplan-Meier dataset. The lack of biopsy samples or fresh plasma/serum from patients, together with the limited availability of datasets, prevents more in-depth analyses. Although a multivariate analysis could not be performed due to the limited sample size, these genes merit more comprehensive analysis in future studies.

Concerning the MAPK pathway, in both spheroid lines, we found an enrichment in the "negative regulation of MAPK pathway" (REAC:R-HSA-5675221) and "RAF-independent MAPK1/3 activation" (REAC:R-HSA-112409) belonging to the "Reactome Pathways Terms". Within these categories, we identified *DUSP*s, *ADIPOR2,* and *PPP2CA* as targets of commonly downregulated miR-1283 and miR-2113 (Fig. S1) (Zhou et al., 2023).

Focusing on the "unique" miRNAs (i.e., those associated with a single cell line) and targeting shared predicted targets, in Mz-ChA-1 3D cells, we found upregulation of miR-98-5p and downregulation of let-7e-5p, let-7i, and let-7f-5p. In these cells, a limitation is the reduced sample size for the spheroids condition ($n = 2$), following quality control exclusion, which may affect the reliability of variance estimation and differential expression results for this specific cell line. For this reason, Mz-ChA-1-specific findings should be interpreted cautiously and require validation in larger experimental sets.

The set of miR-20a-5p, miR-24-3p, miR-30d-5p, and let-7e-5p was validated using an ELISA assay. This technology has been described in technical documentation provided by the manufacturer and in project reports (e.g., European H2020 project descriptions, grant agreement ID 876715), which highlight its high sequence specificity and rapid analysis workflow designed for miRNA quantification across diverse sample types. According to the manufacturer's technical documentation and previously reported applications, the assay shows a sensitivity in the low nanomolar range and high sequence specificity due to probe design targeting mature miRNA sequences, with limited cross-reactivity among closely related family members. Compared with RT-qPCR, the method avoids biases related to reverse transcription efficiency and amplification variability, providing good intra-assay reproducibility and operator-independent readout. The ELISA-based platform has been more recently introduced and has not yet undergone widespread multicenter validation. Therefore, in the present study, it was used as a complementary validation approach to confirm expression trends observed in the microarray analysis rather than as a replacement for RT-qPCR. Notably, miR-20a-5p, and miR-30 family members (and additional miR-146a-5p), identified in our analysis, have also been reported as dysregulated in circulating miRNA profiles of CCA patients, reinforcing their potential role as key regulators of tumor progression and candidate biomarkers (Chaijaroenkul et al., 2026).

In Sk-ChA-1 spheroid cells, the increase of miR-181c-5p, miR-200b-3p, and miR-30d-5p is in agreement with the literature (Meng et al., 2006; Jalil et al., 2023; Han et al., 2020). Notably, miR-181c and miR-200b have been implicated in promoting cancer cell growth and aggressiveness, as well as in modulating the MAPK signaling pathway (Meng et al., 2006). Consistent with our data, Han et al. (2020) demonstrated that miR-30d-5p is significantly upregulated in bile samples from CCA patients compared to those with benign biliary disease. This finding corroborates our results and may aid clinicians to distinguish malignant from benign biliary conditions, further highlighting the role of deregulated miRNAs in CCA pathogenesis.

We also analyzed the expression of predicted targets recognized by multiple miRNAs. Among them, we point out *SMARCAD1*, which is reported to display genome stabilization function, promoting invasion and metastasis diffusion in aggressive phenotypes of breast cancer (Lo et al., 2021; Al Kubaisy et al., 2016) and *HMGA2*. Notably, the latter is upregulated in poorly differentiated, invasive eCCA and metastatic lymph nodes, especially associated with advanced stages. So high levels of HMGA2 correlate with poor survival of patients (Liu et al., 2019). Similarly, it occurs in iCCA (Lee et al., 2014) and in pCCA is reported as a

prognostic marker (Pawaskar et al., 2024). Again, *ATG14*, encoding a key regulator of cell growth promoting autophagy-mediated proliferation, is downregulated by miRNA-424a-5p and upregulated by circCBFB, acting as a sponge of miR-424-5p (Zhao et al., 2022). While this mechanism has been described in HCC, miR-424a-5p also plays a regulatory role in CCA (Wu et al., 2019). Accordingly, we detected downregulation of miRNA-424a-5p in Sk-ChA-1 cells, suggesting a potential derepression of its targets. Another relevant factor is CLOCK, which deserves a special mention for its involvement in CCA mouse models (Mteyrek et al., 2017), emphasizing the potential role of circadian rhythm regulation in cancer development, progression, and metastatic dissemination (Han et al., 2021; Fekry and Eckel-Mahan, 2022). CLOCK is reported among the predicted targets of miR-19b-3p, so we carried out transfection experiments in 2D Sk-ChA-1 cells using antimir-19b-3p, demonstrating an increase in *CLOCK*. In the same treated samples, we detected increased levels of *VIM* and *BMPR2*. Both VIM, a key regulator of cytoskeletal organization and cellular plasticity, and BMPR2, a key component of the BMP/TGF-β signaling axis activating canonical SMAD1/5/8 pathways as well as non-canonical cascades (including MAPK and PI3K/AKT), promote EMT and enhance migration and invasiveness. In 3D spheroid models, its modulation consists of a role in EMT-like plasticity and adaptation to the tumor microenvironment. Notably, miR-19b-3p has already been reported to suppress targets such as CCDC6, supporting its role in driving aggressive tumor behavior of iCCA (Tang et al., 2020). A possible interesting link emerged between miR-19b-3p and another predicted target, *PIK3CA*. In Sk-ChA-1 cells, their inverse expression pattern suggests a potential relief of post-transcriptional repression in spheroids. Although direct validation of the miRNA–target interaction was not performed, it is biologically plausible and aligns with previous evidence indicating that miR-19b-3p may be involved in the PI3K/AKT signaling pathway. Among the high-confidence predicted targets of miR-19b-3p (miRDB score $\geqslant$ 98%) upregulated in Sk-ChA-1 spheroids, we also detected *BMPR2* and *SKIL* (EMT-related), *RPS6KA5* (MAPK-associated), and *RORA* (stress-adaptive transcription). This is consistent with potential derepression mechanisms (Jin et al., 2018). In line with our data, miR-19b-3p, a member of the miR-17-92 cluster, promotes CCA growth by modulating PTEN and IL-6/STAT3 signaling, supporting a role for shared miRNAs in coordinating key oncogenic pathways, including PI3K/AKT and MAPK, in eCCA (Zhu et al., 2014). Furthermore, 3D Sk-ChA-1 displayed high levels of *CDKN1B*, a putative target of the downregulated miR-221-3p.

Finally, we observed upregulation of TNRC6B, a regulatory factor binding the Ago complex, and recruiting RNAs to P-bodies (Baillat and Shiekhattar, 2009), which is emerging as involved in cancer. Joyce et al. (2018) reported that epigenetic alterations in miRNA-processing genes, including proteins interacting with the Ago complex, such as TNRC6B, can affect miRNA biogenesis and are associated with elevated cancer risk. This emphasizes their regulatory functional role in tumorigenesis.

These investigations on dysregulated miRNAs and their predicted targets in spheroids compared with monolayer cells in eCCA shed light on the pathways potentially driving the transition between culture conditions. Such differences between the two conditions may reflect key molecular events underlying different stages of tumor aggressiveness and the enhanced propensity for dissemination, suggesting new perspectives, derived from a more accurate in vivo-like model.

Even though this study is entirely preclinical, the reproducible modulation of PI3K/AKT and MAPK/ERK signaling observed under 3D conditions, supported by phosphorylation analyses and alterations in pathway-related gene expression, identifies biologically and pharmacologically relevant targetable signaling axes, although it requires additional functional and therapeutic exploration, including assays such as autophagic flux measurements or direct pathway modulation studies, not performed in this study. Nevertheless, these miRNAs may be relevant for developing new blocking molecules by gene therapy or pharmacological approaches, given the availability of pharmacological inhibitors targeting PI3K/AKT and MAPK/ERK pathways to further validate their potential.

Supplementary data to this article can be found online at https://doi.org/10.1016/j.yexmp.2026.105059.

CRediT authorship contribution statement

Leda Roncoroni: Writing – review & editing, Writing – original draft, Supervision, Funding acquisition, Data curation, Conceptualization. **Anna Terrazzan:** Writing – review & editing, Writing – original draft, Validation, Software, Methodology, Investigation, Conceptualization. **Luca Elli:** Resources, Investigation, Conceptualization. **Pietro Ancona:** Software. **Paula Olaizola:** Resources, Methodology. **Silvia Tabano:** Methodology. **Patrizia Colapietro:** Methodology. **Filippo Gamberini:** Software, Methodology. **Chiara Orlandi:** Methodology. **Gianluca Aguiari:** Visualization, Validation. **Cristian Taccioli:** Visualization, Investigation, Formal analysis. **Luisa Doneda:** Visualization, Resources. **Nicoletta Bianchi:** Writing – review & editing, Writing – original draft, Supervision, Project administration, Investigation, Funding acquisition, Data curation, Conceptualization.

Ethics statement

Not applicable. This study has been conducted using only in vitro cell culture models.

Funding

This research was supported by Fondo di Ateneo per la Ricerca (FAR 2022, application n.730973 to N.B.), and partially funded by the Italian Ministry of Health, Current research IRCCS (to L.R.).

Declaration of competing interest

The authors declare that they have no known competing financial interests or personal relationships that could have appeared to influence the work reported in this paper.

Acknowledgements

We thank Co.Pe.Go. (Soc.Coop.O.P.) for the liberal voluntary contribution to this project, Dr. Luke Boulter for gently providing the Sk-ChA-1 cell line, and Dr. Cristina Zuccato for the technical help provided.

Data availability

The data that supports the findings of this study are available in the supplementary material of this article. Supplementary data to this article can be found online at https://doi.org/10.1016/j.yexmp.2026.105059. Raw data are available on request from the authors.

References

Al Kubaisy, E., Arafat, K., De Wever, O., Hassan, A.H., Attoub, S., 2016. SMARCAD1 knockdown uncovers its role in breast cancer cell migration, invasion, and metastasis. Expert Opin. Ther. Targets 20, 1035–1043. https://doi.org/10.1080/14728222.2016.1195059.

Alpini, G., McGill, J.M., Larusso, N.F., 2002. The pathobiology of biliary epithelia. Hepatology 35, 1256–1268. https://doi.org/10.1053/jhep.2002.33541.

Arnoff, T.E., El-Deiry, W.S., 2022. MDM2/MDM4 amplification and CDKN2A deletion in metastatic melanoma and glioblastoma multiforme may have implications for targeted therapeutics and immunotherapy. Am. J. Cancer Res. 12, 2102–2117.

Baillat, D., Shiekhattar, R., 2009. Functional dissection of the human TNRC6 (GW182-related) family of proteins. Mol. Cell. Biol. 29, 4144–4155. https://doi.org/10.1128/MCB.00380-09.

Banales, J.M., Marin, J.J.G., Lamarca, A., Rodrigues, P.M., Khan, S.A., Roberts, L.R., Cardinale, V., Carpino, G., Andersen, J.B., Braconi, C., Calvisi, D.F., Perugorria, M.J., Fabris, L., Boulter, L., Macias, R.I.R., Gaudio, E., Alvaro, D., Gradilone, S.A., Strazzabosco, M., Marzioni, M., Coulouarn, C., Fouassier, L., Raggi, C., Invernizzi, P., Mertens, J.C., Moncsek, A., Ilyas, S.I., Heimbach, J., Koerkamp, B.G., Bruix, J.,

Forner, A., Bridgewater, J., Valle, J.W., Gores, G.J., 2020. Cholangiocarcinoma 2020: the next horizon in mechanisms and management. Nat. Rev. Gastroenterol. Hepatol. 17, 557–588. https://doi.org/10.1038/s41575-020-0310-z.
Bortoletto, A.S., Parchem, R.J., 2023. KRAS hijacks the miRNA regulatory pathway in Cancer. Cancer Res. 83, 1563–1572. https://doi.org/10.1158/0008-5472.CAN-23-0296.
Boyer, B., Tucker, G.C., Vallés, A.M., Franke, W.W., Thiery, J.P., 1989. Rearrangements of desmosomal and cytoskeletal proteins during the transition from epithelial to fibroblastoid organization in cultured rat bladder carcinoma cells. J. Cell Biol. 109, 1495–1509. https://doi.org/10.1083/jcb.109.4.1495.
Chaijaroenkul, W., Charoenkajonchai, S., Tongsiri, N., Na-Bangchang, K., 2026. Circulating microRNAs expression as prognosis biomarker of cholangiocarcinoma. Asian Pac. J. Cancer Prev. 27, 307–317. https://doi.org/10.31557/APJCP.2026.27.1.307.
Chandrashekar, D.S., Karthikeyan, S.K., Korla, P.K., Patel, H., Shovon, A.R., Athar, M., Netto, G.J., Qin, Z.S., Kumar, S., Manne, U., Creighton, C.J., Varambally, S., 2022. UALCAN: an update to the integrated cancer data analysis platform. Neoplasia 25, 18–27. https://doi.org/10.1016/j.neo.2022.01.001.
Chen, Y., Wang, X., 2020. miRDB: an online database for prediction of functional microRNA targets. Nucleic Acids Res. 48, 127–131. https://doi.org/10.1093/nar/gkz757.
Chen, H., Zhang, Y., Su, H., Shi, H., Xiong, Q., Su, Z., 2019. Overexpression of miR-1283 inhibits cell proliferation and invasion of glioma cells by targeting ATF4. Oncol. Res. 27, 325–334. https://doi.org/10.3727/096504018X152512820868.
Chhichholiya, Y., Singh, H.V., Vashistha, R., Singh, S., Munshi, A., 2024. Deciphering the role of KRAS gene in oncogenesis: focus on signaling pathways, genetic alterations in 3'UTR, KRAS specific miRNAs and therapeutic interventions. Crit. Rev. Oncol. Hematol. 194, 104250. https://doi.org/10.1016/j.critrevonc.2023.104250.
Delarue, M., Montel, F., Vignjevic, D., Prost, J., Joanny, J.F., Cappello, G., 2014. Compressive stress inhibits proliferation in tumor spheroids through a volume limitation. Biophys. J. 107, 1821–1828. https://doi.org/10.1016/j.bpj.2014.08.031.
DiPeri, T.P., Zhao, M., Evans, K.W., Varadarajan, K., Moss, T., Scott, S., Kahle, M.P., Byrnes, C.C., Chen, H., Lee, S.S., Halim, A.B., Hirai, H., Wacheck, V., Kwong, L.N., Rodon, J., Javle, M., Meric-Bernstam, F., 2024. Convergent MAPK pathway alterations mediate acquired resistance to FGFR inhibitors in FGFR2 fusion-positive cholangiocarcinoma. J. Hepatol. 80, 322–334. https://doi.org/10.1016/j.jhep.2023.10.041.
Dolfini, E., Elli, L., Roncoroni, L., Costa, B., Colleoni, M.P., Lorusso, V., Ramponi, S., Braidotti, P., Ferrero, S., Falini, M.L., Bardella, M.T., 2005a. Damaging effects of gliadin on three-dimensional cell culture model. World J. Gastroenterol. 11, 5973–5977. https://doi.org/10.3748/wjg.v11.i38.5973.
Dolfini, E., Roncoroni, L., Elli, L., Fumagalli, C., Colombo, R., Ramponi, S., Forlani, F., Bardella, M.T., 2005b. Cytoskeleton reorganization and ultrastructural damage induced by gliadin in a three-dimensional in vitro model. World J. Gastroenterol. 11, 7597–7601. https://doi.org/10.3748/wjg.v11.i48.7597.
Ehrlich, L., Hall, C., Venter, J., Dostal, D., Bernuzzi, F., Invernizzi, P., Meng, F., Trzeciakowski, J.P., Zhou, T., Standeford, H., Alpini, G., Lairmore, T.C., Glaser, S., 2017. miR-24 inhibition increases menin expression and decreases cholangiocarcinoma proliferation. Am. J. Pathol. 187, 570–580. https://doi.org/10.1016/j.ajpath.2016.10.021.
Elli, L., Roncoroni, L., Doneda, L., Ciulla, M.M., Colombo, R., Braidotti, P., Bonura, A., Bardella, M.T., 2011. Imaging analysis of the gliadin direct effect on tight junctions in an in vitro three-dimensional Lovo cell line culture system. Toxicol. in Vitro 25, 45–50. https://doi.org/10.1016/j.tiv.2010.09.005.
Fekry, B., Eckel-Mahan, K., 2022. The circadian clock and cancer: links between circadian disruption and disease pathology. J. Biochem. 171, 477–486. https://doi.org/10.1093/jb/mvac017.
Han, Y., Meng, F., Venter, J., Wu, N., Wan, Y., Standeford, H., Francis, H., Meininger, C., Greene Jr., J., Trzeciakowski, J.P., Ehrlich, L., Glaser, S., Alpini, G., 2016. miR-34a-dependent overexpression of Per1 decreases cholangiocarcinoma growth. J. Hepatol. 64, 1295–1304. https://doi.org/10.1016/j.jhep.2016.02.024.
Han, H.S., Kim, M.J., Han, J.H., Yun, J., Kim, H.K., Yang, Y., Kim, K.B., Park, S.M., 2020. Bile-derived circulating extracellular miR-30d-5p and miR-92a-3p as potential biomarkers for cholangiocarcinoma. Hepatobiliary Pancreat. Dis. Int. 19, 41–50. https://doi.org/10.1016/j.hbpd.2019.10.009.
Han, Y., Chen, L., Baiocchi, L., Ceci, L., Glaser, S., Francis, H., Alpini, G., Kennedy, L., 2021. Circadian rhythm and melatonin in liver carcinogenesis: updates on current findings. Crit. Rev. Oncog. 26, 69–85. https://doi.org/10.1615/CritRevOncog.2021039881.
Han, M., Yamaguchi, S., Onishi, M., Fujii, T., Hosoya, M., Wen, X., Kido, H., Kato, S., 2022. The MDM2 and CDKN2A copy-number-variation influence the TP53-signature-score in wild-type TP53 luminal type breast cancer. Anticancer Res. 42, 2277–2288. https://doi.org/10.21873/anticanres.15707.
Hellemans, J., Mortier, G., De Paepe, A., Speleman, F., Vandesompele, J., 2007. qBase relative quantification framework and software for management and automated analysis of real-time quantitative PCR data. Genome Biol. 8, R19. https://doi.org/10.1186/gb-2007-8-2-r19.
Hu, Z.G., Zheng, C.W., Su, H.Z., Zeng, Y.L., Lin, C.J., Guo, Z.Y., Zhong, F.D., Yuan, G.D., He, S.Q., 2019. MicroRNA-329-mediated PTTG1 downregulation inactivates the MAPK signaling pathway to suppress cell proliferation and tumor growth in cholangiocarcinoma. J. Cell. Biochem. 120, 9964–9978. https://doi.org/10.1002/jcb.28279.
Isomoto, H., Kobayashi, S., Werneburg, N.W., Bronk, S.F., Guicciardi, M.E., Frank, D.A., Gores, G.J., 2005. Interleukin 6 upregulates myeloid cell leukemia-1 expression through a STAT3 pathway in cholangiocarcinoma cells. Hepatology 42, 1329–1338. https://doi.org/10.1002/hep.20966.
Jalil, A.T., Abdulhadi, M.A., Al-Ameer, L.R., Khaleel, L.A., Abdulameer, S.J., Hadi, A.M., Merza, M.S., Zabibah, R.S., Ali, A., 2023. Small but mighty: how microRNAs drive the deadly progression of cholangiocarcinoma. Pathol. Res. Pract. 247, 154565. https://doi.org/10.1016/j.prp.2023.154565.
Jin, J., Sun, Z., Yang, F., Tang, L., Chen, W., Guan, X., 2018. miR-19b-3p inhibits breast cancer cell proliferation and reverses saracatinib-resistance by regulating PI3K/Akt pathway. Arch. Biochem. Biophys. 645, 54–60. https://doi.org/10.1016/j.abb.2018.03.015.
Joyce, B.T., Zheng, Y., Zhang, Z., Liu, L., Kocherginsky, M., Murphy, R., Achenbach, C.J., Musa, J., Wehbe, F., Just, A., Shen, J., Vokonas, P., Schwartz, J., Baccarelli, A.A., Hou, L., 2018. miRNA-processing gene methylation and cancer risk. Cancer Epidemiol. Biomarkers Prev. 27, 550–557. https://doi.org/10.1158/1055-9965.EPI-17-0849.
Kang, K.J., Pyo, J.H., Ryu, K.J., Kim, S.J., Ha, J.M., Choi, K., Hong, S.N., Min, B.H., Chang, D.K., Son, H.J., Rhee, P.L., Kim, J.J., Kim, Y.H., 2015. Oncogenic role of BOLL in colorectal cancer. Dig. Dis. Sci. 60, 1663–1673. https://doi.org/10.1007/s10620-015-3533-z.
Karlsen, T.H., Folseraas, T., Thorburn, D., Vesterhus, M., 2017. Primary sclerosing cholangitis– a comprehensive review. J. Hepatol. 67, 1298–1323. https://doi.org/10.1016/j.jhep.2017.07.022.
Khan, S.A., Thomas, H.C., Davidson, B.R., Taylor-Robinson, S.D., 2005. Cholangiocarcinoma. Lancet 366, 1303–1314. https://doi.org/10.1016/S0140-6736(05)67530-7.
Knuth, A., Gabbert, H., Dippold, W., Klein, O., Sachsse, W., Bitter-Suermann, D., Prellwitz, W., Meyer zum Büschenfelde, K.H., 1985. Biliary adenocarcinoma. Characterisation of three new human tumor cell lines. J. Hepatol. 1, 579–596. https://doi.org/10.1016/s0168-8278(85)80002-7.
LaRue, K.E., Khalil, M., Freyer, J.P., 2004. Microenvironmental regulation of proliferation in multicellular spheroids is mediated through differential expression of cyclin-dependent kinase inhibitors. Cancer Res. 64, 1621–1631. https://doi.org/10.1158/0008-5472.can-2902-2.
Lee, C.T., Wu, T.T., Lohse, C.M., Zhang, L., 2014. High-mobility group AT-hook 2: an independent marker of poor prognosis in intrahepatic cholangiocarcinoma. Hum. Pathol. 45, 2334–2340. https://doi.org/10.1016/j.humpath.2014.04.026.
Li, W., Li, M., Su, X., Qin, L., Miao, M., Yu, C., Shen, Y., Luo, Q., Chen, Q., 2014. Mycoepoxydiene induces apoptosis and inhibits TPA-induced invasion in human cholangiocarcinoma cells via blocking NF-κB pathway. Biochimie 101, 183–191. https://doi.org/10.1016/j.biochi.2014.01.012.
Li, S., Chen, J., Fan, Y., Xu, X., Xiong, M., Qi, Y., Wu, W., Zhao, Y., 2022. CircZNF91 promotes the malignant phenotype of chronic lymphocytic leukemia cells by targeting the miR-1283/WEE1 axis. Biomed. Res. Int., 2855394 https://doi.org/10.1155/2022/2855394.
Liu, R., Yang, Z., Huang, S., Li, D., Zou, Q., Yuan, Y., 2019. The expressions of HMGA2 and Thy1 in extrahepatic cholangiocarcinoma and their clinicopathological significances. Surg. Oncol. 29, 41–47. https://doi.org/10.1016/j.suronc.2019.01.013.
Lo, C.S.Y., van Toorn, M., Gaggioli, V., Paes Dias, M., Zhu, Y., Manolika, E.M., Zhao, W., van der Does, M., Mukherjee, C., Souto Gonçalves, J.G.S.C., van Royen, M.E., French, P.J., Demmers, J., Smal, I., Lans, H., Wheeler, D., Jonkers, J., Chaudhuri, A. R., Marteijn, J.A., Taneja, N., 2021. SMARCAD1-mediated active replication fork stability maintains genome integrity. Sci. Adv. 7, eabe7804. https://doi.org/10.1126/sciadv.abe7804.
Meng, F., Henson, R., Lang, M., Wehbe, H., Maheshwari, S., Mendell, J.T., Jiang, J., Schmittgen, T.D., Patel, T., 2006. Involvement of human micro-rna in growth and response to chemotherapy in human cholangiocarcinoma cell lines. Gastroenterology 130, 2113–2129. https://doi.org/10.1053/j.gastro.2006.02.057.
Ming, M., Ying, M., Ling, M., 2019. miRNA-125a-5p inhibits hepatocellular carcinoma cell proliferation and induces apoptosis by targeting TP53 regulated inhibitor of apoptosis 1 and Bcl-2-like-2 protein. Exp. Ther. Med. 18, 1196–1202. https://doi.org/10.3892/etm.2019.7674.
Mischiati, C., Ura, B., Roncoroni, L., Elli, L., Cervellati, C., Squerzanti, M., Conte, D., Doneda, L., Polverino de Laureto, P., de Franceschi, G., Calza, R., Barrero, C.A., Merali, S., Ferrari, C., Bergamini, C.M., Agostinelli, E., 2015. Changes in protein expression in two cholangiocarcinoma cell lines undergoing formation of multicellular tumor spheroids in vitro. PLoS One 10, e0118906. https://doi.org/10.1371/journal.pone.0118906.
Mitchell, P.S., Parkin, R.K., Kroh, E.M., Fritz, B.R., Wyman, S.K., Pogosova-Agadjanyan, E.L., Peterson, A., Noteboom, J., O'Briant, K.C., Allen, A., Lin, D.W., Urban, N., Drescher, C.W., Knudsen, B.S., Stirewalt, D.L., Gentleman, R., Vessella, R. L., Nelson, P.S., Martin, D.B., Tewari, M., 2008. Circulating microRNAs as stable blood-based markers for cancer detection. Proc. Natl. Acad. Sci. USA 105, 10513–10518. https://doi.org/10.1073/pnas.0804549105.
Montal, R., Sia, D., Montironi, C., Leow, W.Q., Esteban-Fabró, R., Pinyol, R., Torres-Martin, M., Bassaganyas, L., Moeini, A., Peix, J., Cabellos, L., Maeda, M., Villacorta-Martin, C., Tabrizian, P., Rodriguez-Carunchio, L., Castellano, G., Sempoux, C., Minguez, B., Pawlik, T.M., Labgaa, I., Roberts, L.R., Sole, M., Fiel, M.I., Thung, S., Fuster, J., Roayaie, S., Villanueva, A., Schwartz, M., Llovet, J.M., 2020. Molecular classification and therapeutic targets in extrahepatic cholangiocarcinoma. J. Hepatol. 73, 315–327. https://doi.org/10.1016/j.jhep.2020.03.008.
Mteyrek, A., Filipski, E., Guettier, C., Oklejewicz, M., van der Horst, G.T., Okyar, A., Lévi, F., 2017. Critical cholangiocarcinogenesis control by cryptochrome clock genes. Int. J. Cancer 140, 2473–2483. https://doi.org/10.1002/ijc.30663.
Pawaskar, R., Huang, K.Z., Pham, H., Nagrial, A., Wong, M., O'Neill, S., Pleass, H., Yuen, L., Lam, V.W.T., Richardson, A., Pang, T., Nahm, C.B., 2024. Systematic review of preoperative prognostic biomarkers in perihilar cholangiocarcinoma. Cancers (Basel) 16, 698. https://doi.org/10.3390/cancers16040698.

Prinz, C., Frese, R., Grams, M., Fehring, L., 2022. Emerging role of microRNA dysregulation in diagnosis and prognosis of extrahepatic cholangiocarcinoma. Genes (Basel) 13, 1479. https://doi.org/10.3390/genes13081479.
Prior, I.A., Lewis, P.D., Mattos, C., 2012. A comprehensive survey of Ras mutations in cancer. Cancer Res. 72, 2457–2467. https://doi.org/10.1158/0008-5472.CAN-11-2612.
Qian, J., Chen, C., Zhao, C., Xu, X., Xu, Y., Zhang, Y., Qian, C., 2023. Hsa_circRNA_0084043 promoting tumorigenesis in glioma through miR-577 sponging. Heliyon 9, e19219. https://doi.org/10.1016/j.heliyon.2023.e19219.
Roncoroni, L., Elli, L., Dolfini, E., Erba, E., Dogliotti, E., Terrani, C., Doneda, L., Grimold, M.G., Bardella, M.T., 2008. Resveratrol inhibits cell growth in a human cholangiocarcinoma cell line. Liver Int. 28, 1426–1436. https://doi.org/10.1111/j.1478-3231.2008.01749.x.
Roncoroni, L., Elli, L., Bardella, M.T., Dogliotti, E., Grimoldi, M.G., Viaggi, S., Erba, E., Zunino, A., Doneda, L., 2010. Cytogenetic characterization, and cell cycle analysis of three human colon adenocarcinoma cell lines: comparison between two- and three-dimensional cell culture systems. Cancer Investig. 28, 7–12. https://doi.org/10.3109/07357900802653431.
Roncoroni, L., Elli, L., Braidotti, P., Tosi, D., Vaira, V., Tacchini, L., Lombardo, V., Branchi, F., Scricciolo, A., Doneda, L., 2018. Transglutaminase 2 mediates the cytotoxicity of resveratrol in a human cholangiocarcinoma and gallbladder cancer cell lines. Nutr. Cancer 70, 761–769. https://doi.org/10.1080/01635581.2018.1470648.
Rupaimoole, R., Slack, F.J., 2017. MicroRNA therapeutics: towards a new era for the management of cancer and other diseases. Nat. Rev. Drug Discov. 16, 203–222. https://doi.org/10.1038/nrd.2016.246.
Sadeghi, H., Kohkalani, M., Seyyed Rezaei, S.A., Kargarmonhaser, S., Mahd Gharebagh, F., Nikdouz, A., Hosseini, A., 2026. microRNAs in pancreatic cancer: key modulators of tumor progression and therapeutic resistance. Biomed. Pharmacother. 196, 119100. https://doi.org/10.1016/j.biopha.2026.119100.
Schwarzenbach, H., 2015. The clinical relevance of circulating, exosomal miRNAs as biomarkers for cancer. Expert. Rev. Mol. Diagn. 15, 1159–1169. https://doi.org/10.1586/14737159.2015.1069183.
Shannon, P., Markiel, A., Ozier, O., Baliga, N.S., Wang, J.T., Ramage, D., Amin, N., Schwikowski, B., Ideker, T., 2003. Cytoscape: a software environment for integrated models of biomolecular interaction networks. Genome Res. 13, 2498–2504. https://doi.org/10.1101/gr.1239303.
Sherr, C.J., 2001. The INK4a/ARF network in tumour suppression. Nat. Rev. Mol. Cell Biol. 2, 731–737. https://doi.org/10.1038/35096061.
Shi, L., Magee, P., Fassan, M., Sahoo, S., Leong, H.S., Lee, D., Sellers, R., Brullé-Soumaré, L., Cairo, S., Monteverde, T., Volinia, S., Smith, D.D., Di Leva, G., Galuppini, F., Paliouras, A.R., Zeng, K., O'Keefe, R., Garofalo, M., 2021. A KRAS-responsive long non-coding RNA controls microRNA processing. Nat. Commun. 12, 2038. https://doi.org/10.1038/s41467-021-22337-3.
Shui, B., Beyett, T.S., Chen, Z., Li, X., La Rocca, G., Gazlay, W.M., Eck, M.J., Lau, K.S., Ventura, A., Haigis, K.M., 2023. Oncogenic K-Ras suppresses global miRNA function. Mol. Cell 83, 2509–2523.e13. https://doi.org/10.1016/j.molcel.2023.06.008.
Simanshu, D.K., Nissley, D.V., McCormick, F., 2017. RAS proteins and their regulators in human disease. Cell 170, 17–33. https://doi.org/10.1016/j.cell.2017.06.009.
Sun, P., Zhang, M., Wang, S., He, Y., Lin, C., Tian, Y., Luo, J., Wang, K., 2026. MiR-31 suppresses lung adenocarcinoma cell proliferation through CDK1 and E2F2-mediated cell cycle arrest. Discov. Oncol. 17, 251. https://doi.org/10.1007/s12672-025-04362-6.
Tabano, S., Caldiroli, A., Terrasi, A., Colapietro, P., Grassi, S., Carnevali, G.S., Fontana, L., Serati, M., Vaira, V., Altamura, A.C., Miozzo, M., Buoli, M., 2020. A miRNome analysis of drug-free manic psychotic bipolar patients versus healthy controls. Eur. Arch. Psychiatry Clin. Neurosci. 270, 893–900. https://doi.org/10.1007/s00406-019-01057-2.
Tang, Z., Kang, B., Li, C., Chen, T., Zhang, Z., 2019. GEPIA2: an enhanced web server for large-scale expression profiling and interactive analysis. Nucleic Acids Res. 47, W556–W560. https://doi.org/10.1093/nar/gkz430.
Tang, Y., Yang, J., Wang, Y., Tang, Z., Liu, S., Tang, Y., 2020. MiR-19b-3p facilitates the proliferation and epithelial-mesenchymal transition, and inhibits the apoptosis of intrahepatic cholangiocarcinoma by suppressing coiled-coil domain containing 6. Arch. Biochem. Biophys. 686, 108367. https://doi.org/10.1016/j.abb.2020.108367.
Terrazzan, A., Crudele, F., Corrà, F., Ancona, P., Palatini, J., Bianchi, N., Volinia, S., 2023. Inverse impact of cancer drugs on circular and linear RNAs in breast cancer cell lines. Noncoding RNA 9, 32. https://doi.org/10.3390/ncrna9030032.
Vandesompele, J., De Preter, K., Pattyn, F., Poppe, B., Van Roy, N., De Paepe, A., Speleman, F., 2002. Accurate normalization of real-time quantitative RT-PCR data by geometric averaging of multiple internal control genes. Genome Biol. 3. https://doi.org/10.1186/gb-2002-3-7-research0034.
Wang, J., Vasaikar, S., Shi, Z., Greer, M., Zhang, B., 2017. WebGestalt 2017: a more comprehensive, powerful, flexible and interactive gene set enrichment analysis toolkit. Nucleic Acids Res. 45, W130–W137. https://doi.org/10.1093/nar/gkx356.
Wu, J., Yang, B., Zhang, Y., Feng, X., He, B., Xie, H., Zhou, L., Wu, J., Zheng, S., 2019. miR-424-5p represses the metastasis and invasion of intrahepatic cholangiocarcinoma by targeting ARK5. Int. J. Biol. Sci. 15, 1591–1599. https://doi.org/10.7150/ijbs.34113.
Wu, X., Heng, J., Li, M., Deng, D., Wu, B., Wang, M., Li, S., Gao, S., Qi, Y., Li, E., 2024. The prognostic value of microRNA-200 family expression in digestive system tumors: a meta-analysis and validation. Med. Comm. Oncology 3, e86. https://doi.org/10.1002/mog2.86.
Xia, J., Benner, M.J., Hancock, R.E., 2014. NetworkAnalyst—integrative approaches for protein–protein interaction network analysis and visual exploration. Nucleic Acids Res. 42, W167–W174. https://doi.org/10.1093/nar/gku443.
Yang, Y., Wang, J., Wan, J., Cheng, Q., Cheng, Z., Zhou, X., Wang, O., Shi, K., Wang, L., Wang, B., Zhu, X., Chen, J., Feng, D., Liu, Y., Jahan-Mihan, Y., Haddock, A.N., Edenfield, B.H., Peng, G., Hohenstein, J.D., McCabe, C.E., O'Brien, D.R., Wang, C., Ilyas, S.I., Jiang, L., Torbenson, M.S., Wang, H., Nakhleh, R.E., Shi, X., Wang, Y., Bi, Y., Gores, G.J., Patel, T., Ji, B., 2024. PTEN deficiency induces an extrahepatic cholangitis-cholangiocarcinoma continuum via aurora kinase a in mice. J. Hepatol. 81, 120–134. https://doi.org/10.1016/j.jhep.2024.02.018.
Yin, C., Mou, Q., Pan, X., Zhang, G., Li, H., Sun, Y., 2018. MiR-577 suppresses epithelial-mesenchymal transition and metastasis of breast cancer by targeting Rab25. Thorac. Cancer 9, 472–479. https://doi.org/10.1111/1759-7714.12612.
Yu, H., Liu, Y., Wang, Y., Li, Y., Sun, J., Liu, L., 2022. Circ_0005397 enhances hepatocellular carcinoma progression through miR-1283/HEG1. Ann. Hepatol. 27, 100712. https://doi.org/10.1016/j.aohep.2022.100712.
Zhang, W., Shen, C., Li, C., Yang, G., Liu, H., Chen, X., Zhu, D., Zou, H., Zhen, Y., Zhang, D., Zhao, S., 2016. miR-577 inhibits glioblastoma tumor growth via the Wnt signaling pathway. Mol. Carcinog. 55, 575–585. https://doi.org/10.1002/mc.22304.
Zhang, W., Sun, J., Chen, J., Xu, C., Zhang, L., 2019. Downregulation of miR-95 in gastric cancer promotes EMT via regulation of slug, thereby promoting migration and invasion. Oncol. Rep. 41, 1395–1403. https://doi.org/10.3892/or.2018.6911.
Zhang, L., Chen, Y., Bao, C., Zhang, X., Li, H., 2020. Eukaryotic initiation factor 4AIII facilitates hepatocellular carcinoma cell proliferation, migration, and epithelial-mesenchymal transition process via antagonistically binding to WD repeat domain 66 with miRNA-2113. J. Cell. Physiol. 235, 8199–8209. https://doi.org/10.1002/jcp.29475.
Zhao, Z., He, J., Feng, C., 2022. CircCBFB is a mediator of hepatocellular carcinoma cell autophagy and proliferation through miR-424-5p/ATG14 axis. Immunol. Res. 70, 341–353. https://doi.org/10.1007/s12026-021-09255-8.
Zhou, F., Zeng, L., Chen, X., Zhou, F., Zhang, Z., Yuan, Y., Wang, H., Yao, H., Tian, J., Liu, X., Zhao, J., Huang, X., Pu, J., Cho, W.C., Cao, J., Jiang, X., 2023. DUSP10 upregulation is a poor prognosticator and promotes cell proliferation and migration in glioma. Front. Oncol. 12, 1050756. https://doi.org/10.3389/fonc.2022.1050756.
Zhu, H., Han, C., Lu, D., Wu, T., 2014. miR-17-92 cluster promotes cholangiocarcinoma growth: evidence for PTEN as downstream target and IL-6/Stat3 as upstream activator. Am. J. Pathol. 184, 2828–2839. https://doi.org/10.1016/j.ajpath.2014.06.024.